Chem Soc Rev

Chemical Society Reviews

www.rsc.org/chemsocrev

Volume 36 | Number 11 | November 2007 | Pages 1697–1844

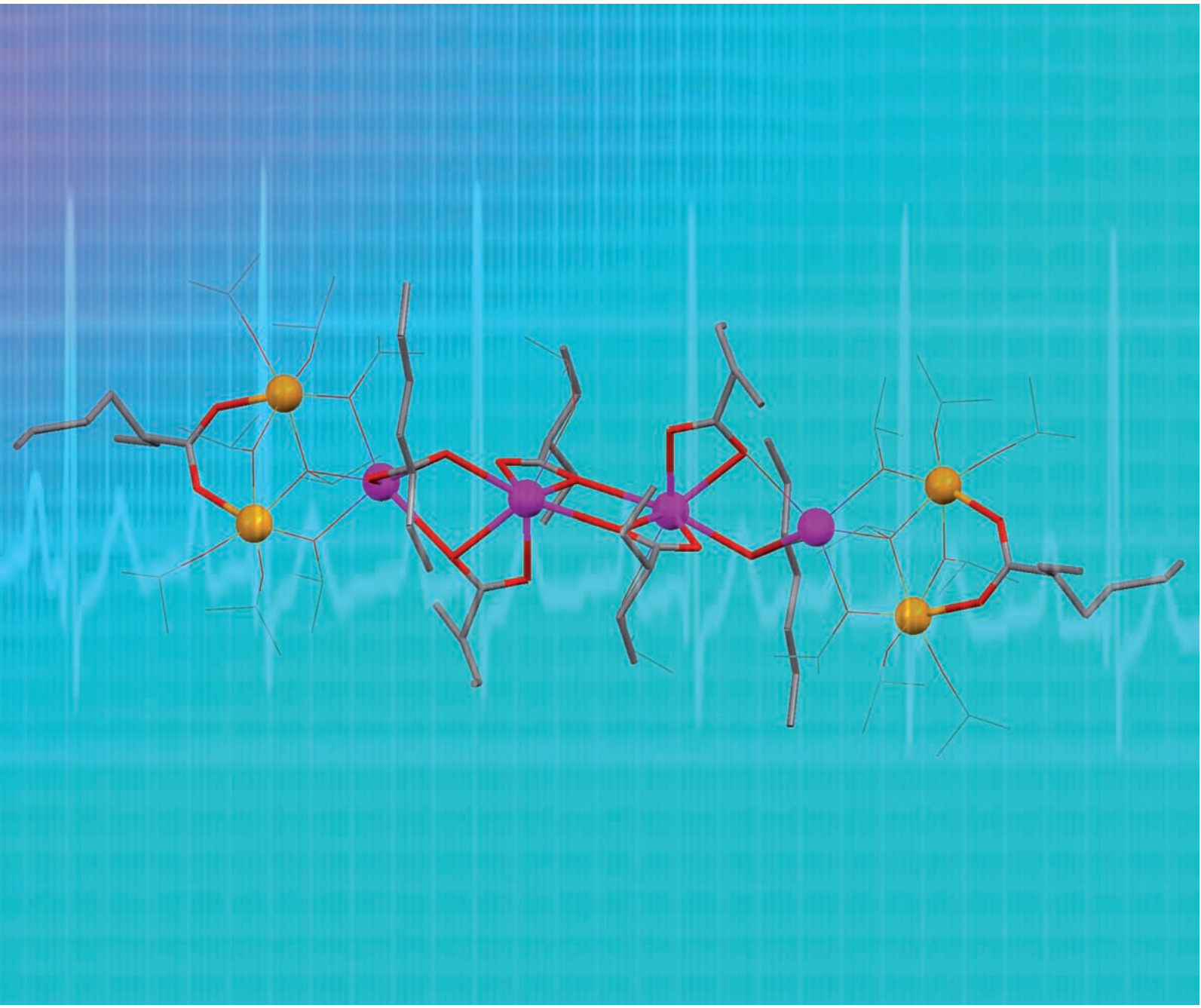

ISSN 0306-0012

CRITICAL REVIEW
Shashank Mishra, Stéphane Daniele and Liliane G. Hubert-Pfalzgraf
Metal 2-ethylhexanoates and related compounds as useful precursors in materials science

TUTORIAL REVIEW
Stephen T. Liddle, Ian S. Edworthy and Polly L. Arnold
Anionic tethered *N*-heterocyclic carbene chemistry

RSC Publishing

Metal 2-ethylhexanoates and related compounds as useful precursors in materials science

Shashank Mishra,* Stéphane Daniele* and Liliane G. Hubert-Pfalzgraf†

Received 5th December 2006
First published as an Advance Article on the web 26th June 2007
DOI: 10.1039/b614334m

This *critical review* deals with the chemistry and applications of metal alkanoates with medium size (C_5 to C_{12}) carbon chain length. A particular emphasis is given to metal 2-ethylhexanoates, which find wide applications as metal–organic precursors in materials science, as catalysts for ring opening polymerizations and also in painting industries for their properties as driers. After a brief introduction and an overview of synthesis, structural and physico-chemical properties, this article discuses extensively the applications of these compounds in materials science. Finally, it identifies and signifies the areas for future research in the looking ahead section. The aim of this review is to bridge the areas of precursor's chemistry and materials science by providing a reference text for researchers working either in or at the interface of these two areas (125 references).

1 Introduction

Binary or multimetallic oxides cover a wide range of applications in electronics, optics, catalysis, magnetism and environmental issues.[1] The development of new, tuneable materials for the technological demands requires flexible routes, which are represented by conventional, hydrolytic or less conventional, non-hydrolytic sol–gel processing and metal organic deposition (MOD) in solution or chemical vapor deposition (CVD) in the vapor phase, all being summarized as ''*Chimie douce*''.[2] Rational design of precursors and optimization of the ligand set require knowledge of the relationships between the properties of the materials and of their precursors, which should thus be structurally well defined.[2] Among the common oxide precursors such as metal β-diketonates, alkanoates and alkoxides, the latter are the most versatile for tailoring properties at a molecular level and conversion into extended arrays by sol–gel method.[3] However, a common problem of the all-alkoxide approach is non-formation of mixed-metal species and thus non-homogeneity at molecular level.[2,3] Unequal hydrolysis and condensation rates of component metal alkoxide in a homogeneous multi-component solution of the metal alkoxides may result in phase separation, leading to higher crystallization temperatures or even undesired crystalline phases. The alkanoate–alkoxide approach overcomes many problems with the all-alkoxide approach. The reaction between an alkoxide and an alkanoate proceeds with the formation of smallest possible aggregate,

Université Claude Bernard Lyon 1, IRCELYON, 2 Avenue A. Einstein, 69626 Villeurbanne Cédex, France.
E-mail: mishrashashank74@rediffmail.com (S.M.); stephane.daniele@ircelyon.univ-lyon1.fr (S.D.);
Fax: +33-4-72-44-53-99; Tel: +33-4-72-44-53-29
† Deceased.

Shashank Mishra

Shashank Mishra was born in Allahabad (U.P.), India in 1974. He received his MSc (1996) and PhD (2002) degrees from the University of Rajasthan, Jaipur (India), and served as a lecturer (2002–2004) at Bundelkhand University, Jhansi (India) before joining (the late) Prof. L. G. Hubert-Pfalzgraf's research laboratory as a post-doctoral fellow in 2004. Since then, he has been working here on homo- and heterometallic molecular precursors for high-tech materials. He has co-authored over two dozen research papers in peer-reviewed international journals and is recipient of a Young Scientist Award of Indian Chemical Society (2004).

Stéphane Daniele

Stéphane Daniele was born in 1969 in Cannes, France. Graduate of the University of Nice–Sophia–Antipolis (France) in 1986, his Master's degree was followed by a PhD in inorganic chemistry (1995) at the University of Nice–Sophia–Antipolis (with Prof. L. G. Hubert-Pfalzgraf) on the synthesis and characterization of molecular precursors for sol–gel processes. He was a Research Fellow (1995–1996, JSPS Grant; 1996–1998, Marie Curie Grant) in the groups of Prof. K. Tanaka at the IMS (Japan) and of Prof. Michael F. Lappert (England), respectively. He is, since 1998, a lecturer at the University of Lyon (France) where he works on various aspects of coordination chemistry and synthesis of functional nanoparticles.

which allows the metals to achieve their most usual coordination number and thus hydrolysis becomes more difficult. Alkanoates act as assembling and oxo donor ligands, and thus have a tendency to increase the nuclearity of the aggregates. Acetates based on divalent metals such as magnesium, cadmium and lead show reactivity toward metal alkoxides and form mixed metal species often in quite mild conditions.[4–7] The selection of a precursor and the solvents is the most important step in the precursor solution approach for the fabrication of thin films *via* MOD. The precursor should have relatively small organic groups in order to minimize the amount of organics to eliminate, and thus minimize the size of the pores and other defects in the film. Short chain metal alkanoates such as acetates are usually insoluble. On the other hand, longer chain alkanoates contain too much organics to produce pure films. Thus, medium sized carbon chain metal alkanoates, such as 2-ethylhexanoates are most suitable precursors for fabricating high quality thin films. Metal 2-ethylhexanoates have other advantages of being inexpensive, air-stable, non-toxic as well as commercially available for a wide number of elements. In contrast to acetate–alkoxide species,[4–7] the chemistry of alkoxide–2-ethylhexanoate precursors is largely unexplored. Recently, the first heterometal alkoxide–alkanoate species involving 2-ethylhexanoate ligands were reported from our laboratory.[8,9] Unlike mixed metal Pb–Ti and Pb–Zr acetate–alkoxides,[4–6] these 2-ethylhexanoate–isopropoxide derivatives $Pb_4Zr_4(\mu\text{-}O_2CCHEtC_4H_9)_4(\mu\text{-}OPr^i)_6(\mu_3\text{-}OPr^i)_2(OPr^i)_8(Pr^iOH)_2$ and $Pb_2Ti_4(\mu\text{-}O_2CCHEtC_4H_9)_4(\mu\text{-}OPr^i)_6(\mu_3\text{-}OPr^i)_2(OPr^i)_8$ show absence of oxo ligands, formulae that correspond to simple adducts and, as required for PZ ceramics, a 1 : 1 ratio of lead and zirconium for Pb–Zr derivative.

Metal alkanoate compounds, often named as metallic soaps, show interesting structural, magnetic, mesomorphic and photochemical properties.[10] They are also of great commercial importance and find variety of applications in important areas such as materials science, catalysis, paint industries, *etc.*[11,12] Additionally, metal derivatives of 2-ethylhexanoic and other medium sized aliphatic acids are also used as fungicides, lubricating agents, stabilizers for plastics, waterproof agents, fuel additives, *etc.*[10]

The present review discuses different aspects such as synthesis, characterisation, physico-chemical properties and applications of medium chain metal alkanoates. A somewhat extensive focus on their applications in materials science is in accordance with the main theme of the article and, in this context, a special emphasis is placed on metal 2-ethylhexanoate derivatives, $[M(O_2CCHEtC_4H_9)_n]_m$.

Liliane G. Hubert-Pfalzgraf

Liliane G. Hubert-Pfalzgraf (1945–2006) was born and educated in Alsace, France. After completing BSc and MSc at the University Louis Pasteur in Strasbourg, she moved to the University of Nice as lecturer with Prof. J. Riess. They launched the laboratoire de Chimie Moléculaire and she received her Doctorat d'Etat. After post-doctoral work at the University of Amsterdam, she returned to the University of Nice–Sophia Antipolis as Professor of Inorganic Chemistry. She joined the faculty of the University Claude Bernard Lyon 1 in 1998. Her major research contributions have been in the field of the design of molecular precursors of oxide and non-oxide materials and understanding their transformations via CSD or MOCVD routes for applications in electronics, catalysis and nanotechnologies. She was a Fellow of the RSC and a member of the Editorial Boards of Dalton Transactions and Polyhedron before her untimely demise on July 18, 2006.

2 Synthesis

2.1 Homometallic derivatives

Two general methods of preparation of metal alkanoates include metathesis and ligand exchange reactions. The commonly used solvents are either water or a mixture of water and alcohol or sometimes even parent alkanoic acids. Some other methods such as direct reactions of the metals with the corresponding alkanoic acids and anodic dissolution have also been used.

2.1.1 Metathesis reactions. The metathesis reaction between an alkali metal alkanoate and a metal salt (eqn (1), n = 5–11[13–23] (usually sulfate or nitrate) has been exploited for the synthesis of alkanoate derivatives of a large number of metals such as manganese, copper, zinc, lead and lanthanides.[13–35] The main advantage is a very high yield, usually 90–95% or more.

$$CuSO_4 + 5H_2O + 2NaO_2CC_nH_{2n+1} \xrightarrow{H_2O} Cu(O_2CC_nH_{2n+1})_2 + Na_2SO_4 + 5H_2O \quad (1)$$

The manganese(II) 2-ethylhexanoate derivative, $Mn[O_2CCH(Et)C_4H_9]_2\cdot H_2O$ is also prepared[24] by the above method. However, due to its air-sensitivity, all manipulations require inert atmosphere. Nitrates of lanthanides, zinc and lead have also been employed for the metathesis reaction (Scheme 1).

A μ_3-oxo trinuclear iron(III) heptanoate, $[Fe_3O(O_2CC_6H_{13})_6(H_2O)_3]NO_3$ has been synthesized by the reaction of iron(III) nitrate with sodium heptanoate.[32] Other metal salts such as chlorides[33] and perchlorates[34] have also been used as starting materials. Where extra pure metal alkanoates are required, ammonium alkanoates are used in place of alkali

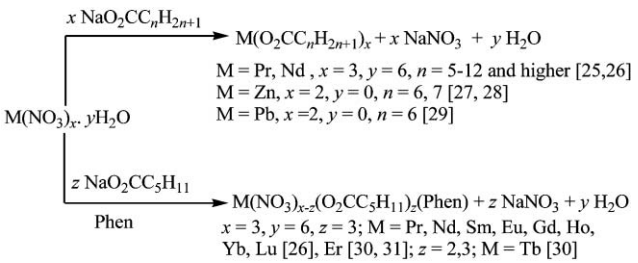

Scheme 1 Synthesis of metal alkanoates from metal nitrates.

metal ones since the unreacted ammonium alkanoate escapes out as gaseous products such as NH_3, NO_2, CO_2 and H_2O on heating. Metal alkanoates of alkaline earth metals, lanthanides and lead have been prepared in high purity and good yield using ammonium alkanoate method.[35]

2.1.2 Ligand exchange reactions. The ligand-exchange reaction between a metal oxide/hydroxide/chloride/acetate (or a higher alkanoate) and an appropriate alkanoic acid is another convenient method for the preparation of metal alkanoate with medium carbon chain length. Metal oxides are preferential starting materials for the synthesis of alkanoates of metals such as copper, zinc, lead, *etc.* (eqn (2)).[36,37]

$$\begin{gathered} MO + 2HO_2CR \xrightarrow[\text{(as a catalyst)}]{\text{acetic acid}} M(O_2CR)_2 + H_2O \\ M = Cu,\ R = C_4H_9,\ C_5H_{11}\ \ [36] \\ M = Zn,\ R = C_5H_{11},\ C_6H_{13},\ C_7H_{15}\ \ [37] \end{gathered} \quad (2)$$

Reaction of an alkanoic acid with a metal hydroxide such as $Zn(OH)_2$, $Sr(OH)_2$,[38] $Co(OH)_2$[39] or carbonates such as $CuCO_3$[40] are similar to that with an oxide (eqn (2)), except that additional H_2O (metal hydroxide) or CO_2 (metal carbonate) are byproducts. Ligand-exchange reactions between metal acetates (or other short chain metal alkanoates) and a slight excess of higher alkanoic acids (eqn (3)) have largely been exploited for the preparation of higher alkanoates of copper, ruthenium, rhodium, molybdenum, *etc.*[33,41–44]

$$M_2(O_2CR)_4X_n + 4R'CO_2H \rightarrow M_2(O_2CR')_4X_n + 4RCO_2H$$

M = Cu, Ru; n = 0; R = CH_3, C_3H_7; R′ = C_4H_9 to $C_{12}H_{25}$ and higher, C_7F_{15};[41]
M = Ru, X = Cl, R′CO_2, dodecyl sulfate; n = 1; R = CH_3, C_3H_7; R′ = C_5H_{11} to $C_{11}H_{23}$ and higher;[42]
M = Mo, Rh, W; n = 0; R = CH_3; R′ = C_4H_9 to $C_{10}H_{21}$, C_7F_{15}[33,43,44] (3)

2-Ethylhexanoate derivatives of alkaline earth metals such as strontium and barium have also been synthesized from their acetates.[45] The ligand-exchange reaction between a metal halide and an alkanoic acid requires the use of triethylamine in order to trap hydrogen chloride.[25] An excess of alkanoic acid is also required in order to avoid the formation of alkanoate–halides.[25]

2.1.3 Miscellaneous methods. The reaction between $Mo(CO)_6$ and an excess of an alkanoic acid in a high boiling solvent such as diglyme has been used to prepare Mo(II) alkanoates[33] (eqn (4)). The use of some THF prevented the sublimation of $Mo(CO)_6$ onto the cool parts of the reaction vessel.

$$\begin{gathered} 2MO(CO)_6 + \underset{\text{in excess}}{RCOOH} \xrightarrow{\text{diglyme}} Mo(O_2CR)_4 + 12CO + 2H_2 \\ R = C_4H_9 \text{ to } C_9H_{19} \end{gathered} \quad (4)$$

Mixed-ligand alkanoates such as $[Ti(OCH_3)_2(O_2CC_9H_{19})_2]$[35] and $[Ti(OC_4H_9)_2(O_2CCHEtC_4H_9)_2]$[46] can be prepared from metal alkoxide and alkanoic acids. 2-Ethylhexanoates and octanoates of manganese, iron, nickel, cobalt and copper have been obtained by an anodic dissolution of metal in the presence of respective alkanoic acid, an electrolyte and acetone or acetonitrile as solvents, the cathode being platinum.[47] This method, however, cannot be used for metals such as bismuth and lead, which undergo electrolytic dissolution at the anode. Additionally, the electrolyte contaminates the final solution with chlorine, which preclude the use of the solution in microelectronic applications. An improved process for synthesis of metal 2-ethylhexanoates is the anodic dissolution of metals in a mixture of 2-ethylhexanoic acid, a low weight aliphatic alcohol, and an electrolyte in a cell in which an ion exchange membrane separates anode and cathode compartments.[48]

2.2 Heterometallic derivatives

$Na_2Zn(O_2C_6H_{11})_4$ is obtained by mixing ethanol solutions of sodium hexanoate and zinc hexanoate in a 2 : 1 molar ratio.[49] $Zr_2(OPr^i)_8(HOPr^i)_2$ reacts with $[Pb(O_2CCHEtC_4H_9)_2]_m$ to give $Pb_4Zr_4(O_2CCHEtC_4H_9)_8(OPr^i)_{16}(HOPr^i)_2$[8] (eqn (5)). On the other hand, a species of 1 : 2 stoichiometry $Pb_2Ti_4(O_2CCHEtC_4H_9)_4(OPr^i)_{16}$ was obtained by reacting lead(II) 2-ethylhexanoate with either one or two equivalents of $Ti(OPr^i)_4$ (eqn (6)), the yield having improved in the later case.[8,9]

$$\begin{gathered} 4Pb(O_2CCHEtC_4H_9)_2 + 2Zr_2(OPr^i)_8(HOPr^i)_2 \rightarrow \\ Pb_4Zr_4(O_2CCEtC_4H_9)_8(OPr^i)_{16}(HOPr^i)_2 + 2Pr^iOH \end{gathered} \quad (5)$$

$$\begin{gathered} 2Pb(O_2CCHEtC_4H_9)_2 + 4Ti(OPr^i)_4 \rightarrow \\ Pb_2Ti(O_2CCHEtC_4H_9)_4(OPr^i)_{16} \end{gathered} \quad (6)$$

3 Characterization

3.1 X-Ray crystallography

Metal alkanoates can be structurally a very diverse group of coordination compounds due to the various coordination modes of the alkanoate ligands (Scheme 2). However,

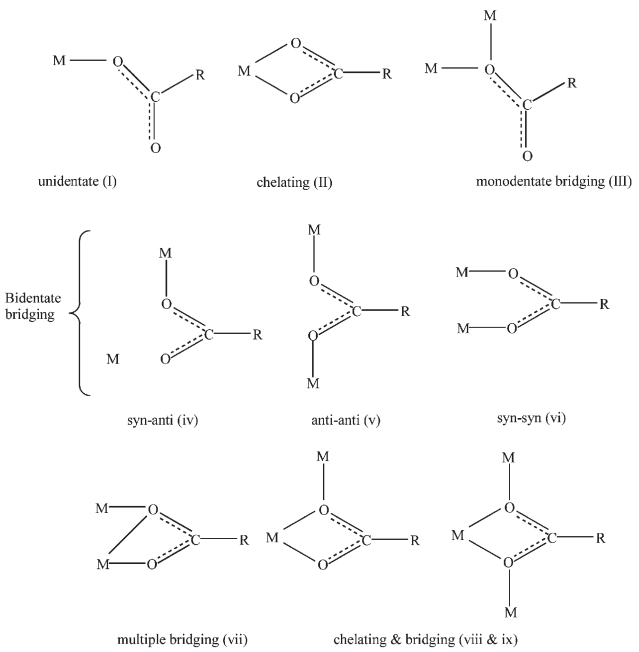

Scheme 2 Various coordination modes of alkanoate ligands.

single-crystal X-ray data on 2-ethylhexanoate and other higher alkanoate derivatives remain scarce since the long carbon chain favors disorder and, as a result, the obtained crystals are often of poor quality.[8]

3.1.1 Homometallic derivatives.

(a) Divalent metals. Copper(II) alkanoates are the most studied class of metal derivatives of medium chain length alkanoic acids because of their important properties as pharmaceutical agents, fungicides, catalysts, gas occlusion compounds and agents in solvent extraction processes.[13–23,36,40] These compounds show an interesting and definite pattern of structures (Scheme 3). In general, most of the compounds contain a tetraalkanoato $Cu_2(O_2CR)_4$ core having a typical dimeric paddle-wheel structure. A large number of these complexes without any donor ligands have been reported, all having the polymeric structure $[Cu_2(O_2CR)_4]_\infty$[13,15,36,40] in which dimeric units are linked into chains by the interaction of a Cu ion from one unit with the alkanoate oxygen of a neighbouring dimer (type e). These copper(II) alkanoates react with additional N- and/or O- donor ligands L (L = H_2O, NH_3, urea, py, 2-apy, 4-apy) to form complexes having diverse stereochemistry. On breaking the polymeric structure by adding a ligand in the apical position, either an isolated dinuclear species with additional Lewis base ligands on the apical positions of the central dicopper tetraalkanoate (type c)[14,18–20] or a dimer of the dinuclear units (type d)[23] are formed. By increasing the ligand concentration, monomeric complexes $Cu(O_2CR)_2L_2$ are also formed (often with monodentate coordination modes of the alkanoate ligands), where ligands may be in *cis* (type b) or *trans* positions (type a).[16,17,20–22] The monomeric-dimeric equilibrium of these copper(II) alkanoates in solution has been studied by UV-Vis spectroscopic and isothermal calorimetric titration.[20]

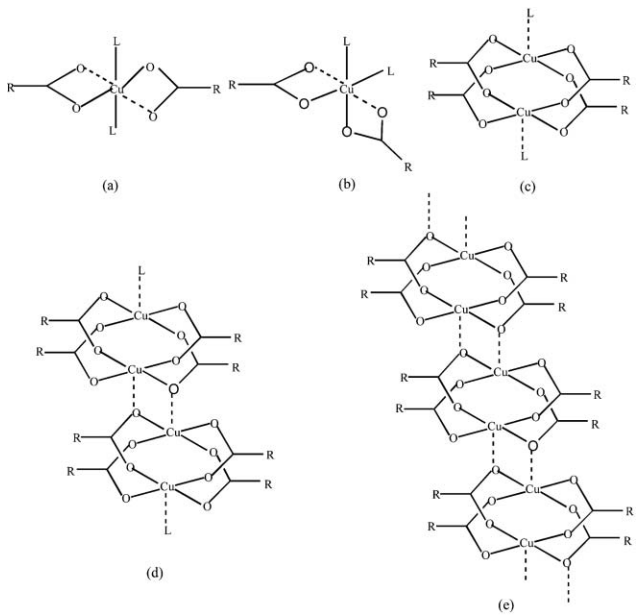

Scheme 3 Different structural types of copper(II) alkanoates: (a) *trans*-mononuclear; (b) *cis*-mononuclear; (c) dinuclear; (d) tetranuclear; and (e) polynuclear.

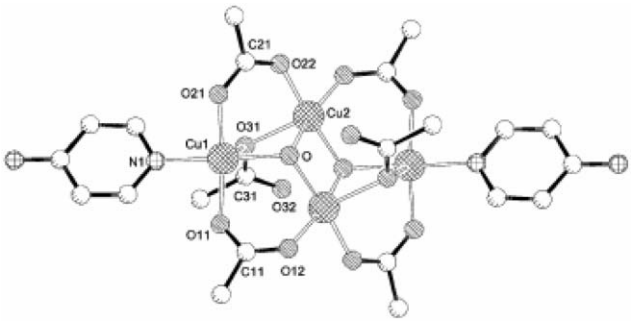

Fig. 1 X-Ray crystal structure of $Cu_4(\mu_3\text{-}OH)_2(\mu,\eta^2\text{-}O_2CC_7H_{15})_4(\mu,\eta^1\text{-}O_2CC_7H_{15})_2(4\text{-apy})_2$. (Reproduced from ref. 22 with permission. Copyright 2002, Royal Society of Chemistry.)

Unlike the reactions of copper(II) hexanoate and heptanoate with 4-aminopyridine (4-apy), which lead to formation of compounds $Cu(O_2CR)_2(4\text{-apy})_2$ (R = C_5H_{11}, C_6H_{13}), a novel, unprecedented centrosymmetric tetranuclear compound $Cu_4(\mu_3\text{-}OH)_2(\mu,\eta^2\text{-}O_2CR)_4(\mu,\eta^1\text{-}O_2CR)_2(4\text{-apy})_2$ (R = C_7H_{15}) has been isolated with copper(II) octanoate.[22] In the structure of this compound, two crystallographically independent copper ions possess distorted square pyramidal coordination (Fig. 1). Three independent octanoate groups are present in the molecule, two of which form bridges from the basal position of one copper ion to the basal site of the second copper ion. The third octanoate anion is bound as a monoatomic bridging ligand to the apical position, shared by both polyhedra. 4-Aminopyridine is coordinated to Cu1 only and occupies one of the basal positions. The distance between the symmetry related hydroxo-bridged Cu2 atoms is 2.89(2) Å, while the Cu1 and Cu2, bridged through alkanoate groups are separated by 3.07(2) to 3.30(1) Å. These distances are much longer than the average Cu···Cu separation reported for tetraalkanoato bridged dimeric compounds.[14,18–20]

$[Zn(\mu,\eta^1\text{:}\eta^1\text{-}O_2CR)_2]_{2\infty}$ (R = C_5H_{11},[37] C_6H_{13},[27] C_7H_{15}),[28] compounds have two-dimensional sheet structure, where tetrahedral zinc atoms are connected by *syn-anti* alkanoates bridges (Fig. 2). Each sheet is characterized by an internal plane containing Zn^{2+} atoms, surrounded by a tetrahedron of O^{2-}, whereas the alkyl chains protrude from each side of this plane. The stacking mode of the layers varies with the number of carbon atoms in the alkyl chain. For example, the addition

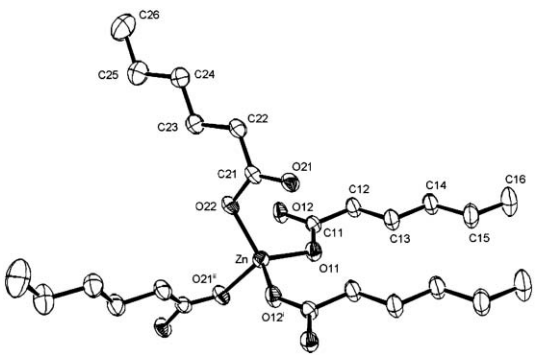

Fig. 2 X-Ray crystal structure of $[Zn(\mu,\eta^1\text{:}\eta^1\text{-}O_2C_6H_{11})_2]_{2\infty}$ (Reproduced from ref. 37*a* with permission. Copyright 2006, Elsevier).

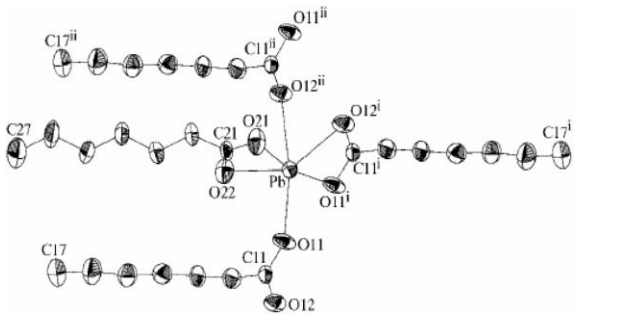

Fig. 3 Structure of $[Pb(\eta^2\text{-}O_2C_7H_{13})(\mu_3,\eta^1\text{:}\eta^1\text{:}\eta^2\text{-}O_2C_7H_{13})]_{2\infty}$ (Reproduced from ref. 29*a* with permission. Copyright 2001, International Union of Crystallography.)

of a carbon atom in going from zinc heptanoate to zinc octanoate results in the structure changing from one in which the planes containing the C_{2n} chains of the two adjacent layers form an angle of approximately 120° to one in which they are parallel.[27,28] The structure of $[Pb(\eta^2\text{-}O_2C_7H_{13})(\mu_3,\eta^1\text{:}\eta^1\text{:}\eta^2\text{-}O_2C_7H_{13})]_{2\infty}$ also consists of two-dimensional layers packed through van der Waals interactions.[29] One of the heptanoate group is chelating [Pb–$O11^i$ 2.58(8), Pb–$O12^i$ 2.73(8)], which also bridges the adjacent Pb atoms along the b direction [Pb–O11 2.56(7), Pb–$O12^{ii}$ 2.62(7)]. The other heptanoate group is only chelating and leads to the shortest Pb–O distances in the structure [Pb–O21 2.45(8), Pb–O22 2.41(9)]. The $6s^2$ lone pair of electrons on Pb^{2+} is stereochemically active leading to a hemidirected octahedral geometry for the O-environment around Pb atoms (Fig. 3).

(b) Trivalent metals. The trinuclear iron(III) heptanoate $[Fe_3(\mu_3\text{-}O)(\mu,\eta^2\text{-}O_2CC_6H_{13})_6(H_2O)_3]NO_3$, has the typical core observed for the structures of $[M_3(\mu_3\text{-}O)(\mu,\eta^2\text{-}O_2CR)_6L_3]^{n+}$ (M = a transition metal, L = ligand or free coordination site), with nearly planar and equilateral Fe_3O group and shortest Fe–O distances known (oxygen being central atom).[32] Over all, it has a double layer structure with an interlamellar orientation of alkyl chains being of a head to head configuration and d_0 interlamellar spacing being 18.2 Å. This compound has been shown to undergo an interesting reversible phase transition at Ts = 225 K. The origin of the transition was interpreted as due to a 60° rotation of the nitrate groups of one sheet out of two of the lamellar structure. The Mössbauer spectroscopic and magnetic moment studies along with the fact that Fe–O distances in the Fe_3O triangles remains approximately constant, indicate that the transformation is not related to the valence trapped phenomena as it has been reported for other trinuclear mixed-valence iron alkanoate complexes $[Fe_3O(O_2CCH_3)_6(3\text{-Cl-py})_3](3\text{-Cl-py})$ and $[Fe_3O(O_2CCH_2CN)_6(H_2O)_3]$.[50]

The 1D-polymeric structure of $[Nd(\mu,\eta^2\text{-}2\text{-ethylhexanoate})_2(\eta^2\text{-}NO_3)(EtOH)_2]_{1\infty}$ have eight-coordinate neodymium centres bridged by two η^2-2-ethylhexanoate ligands. Each neodymium atom is also coordinated to a bidentate nitrate group and two ethanol molecules and the geometry around the metal is a distorted dodecahedron.[51] In contrast, the thulium derivative $[Tm_2(\mu,\eta^3\text{-}O_2C_6H_{11})_2(\mu,\eta^2\text{-}O_2C_6H_{11})_2(\eta^2\text{-}NO_3)_2(\eta^2\text{-phen})_2]$[30] is a dimer in which thulium atoms are held together by two

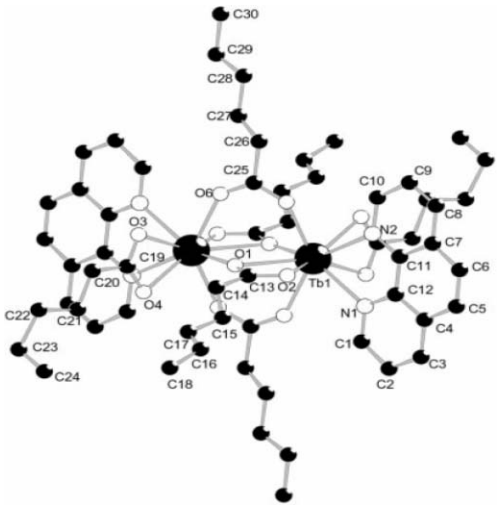

Fig. 4 Structure of $[Tb_2(\mu,\eta^3\text{-}O_2C_6H_{11})_2(\mu,\eta^2\text{-}O_2C_6H_{11})_2(\eta^2\text{-}O_2C_6H_{11})_2(\eta^2\text{-phen})_2]$ (Reproduced from ref. 30 with permission. Copyright 2003, Wiley-VCH.)

bidentate bridging and two tridentate bridging hexanoate groups. The distorted tricapped trigonal prism geometry around thulium atom is completed by bidentate coordinations of nitrate and phenanthroline groups. The tris-hexanoate phenanthroline complexes of lanthanides, $[Ln_2(\mu,\eta^3\text{-}O_2C_6H_{11})_2(\mu,\eta^2\text{-}O_2C_6H_{11})_2(\eta^2\text{-}O_2C_6H_{11})_2(\eta^2\text{-phen})_2]$ (Ln = Pr, Nd, Sm, Tb,[30] Eu)[31] are isostructural with $[Tm_2(\mu,\eta^3\text{-}O_2C_6H_{11})_2(\mu,\eta^2\text{-}O_2C_6H_{11})_2(\eta^2\text{-}NO_3)_2(\eta^2\text{-phen})_2]$, where a bidentate nitrate group is replaced with a bidentate hexanoate group (Fig. 4).

(c) Mixed-valent metals. Mixed-valent metal complexes $[Ru^{II}Ru^{III}(\mu,\eta^2\text{-}O_2C_5H_9)_4Cl]_\infty$[52] and $[Ru^{II}Ru^{III}(\mu,\eta^2\text{-}C_{10}H_{19}O_2)_4(\mu,\eta^2\text{-}C_8H_{17}O_3S)]_\infty$[53] have octahedral ruthenium atoms coordinated by four bridging alkanoate ligands, a Ru–Ru bond and one chloride/octanesulfonate anion. The chloride or octanesulfonate anion bridges the two dinuclear units through axial coordination to form infinite chains. The molecular structure of a mixed-valent cluster of manganese 2-ethylhexanoate compound $[Mn_2^{II}Mn_2^{III}(\mu_3\text{-}O)_2(\mu,\eta^2\text{-}O_2CCHEtC_4H_9)_6(\eta^2\text{-bipy})_2]$ has been reported recently.[24] The two Mn(III) atoms are in a penta-coordinated pure oxygen environment, whereas two other manganese(II) atoms are octahedrally coordinated in a N_2O_4 environment (Fig. 5).

3.1.2 Heterometallic derivatives. The structure of $Na_2[Zn(\eta^1\text{-}O_2C_6H_{11})_4]$ consists of two-dimensional polymeric sheets.[49] Each hexanoate ligand is monodentally coordinated to Zn^{2+}, with O–Zn–O angles [92.5(1)–119.8(1)°] showing large deviations from the regular tetrahedral value of 109.28°. The Zn and Na2 are located on a twofold axis, whereas Na1 resides on a centre of symmetry. Both Na^+ are six-coordinated by O atoms, deformations of the octahedron are larger for the Na1 (Fig. 6).

The basic heterometallic building block (BB) of $Pb_4Zr_4(\mu\text{-}O_2CR')_4(\mu\text{-}OR)_6(\mu_3\text{-}OR)_2(OR)_8(OHR)_2$ (R = Pr^i, R′ = $CHEtC_4H_9$) is a triangular $PbZr_2(OR)_4(\mu\text{-}OR)_3(\mu_3\text{-}OR)(\mu\text{-}O_2CR')$ unit.[8] Two of them are assembled *via* a $Pb_2(O_2CR')_4(OHR)_2$ moiety into a centrosymmetric Pb_4Zr_4 array (Fig. 7).

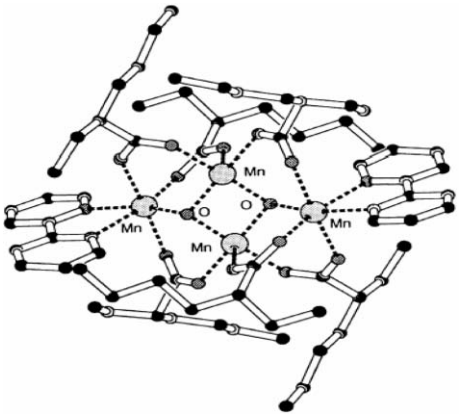

Fig. 5 Structure of $[Mn_2^{II}Mn_2^{III}(\mu_3\text{-}O)_2(\mu,\eta^2\text{-}O_2CCHEtC_4H_9)_6(\eta^2\text{-bipy})_2]$ (Reproduced from ref. 24 with permission. Copyright 2002, Elsevier.)

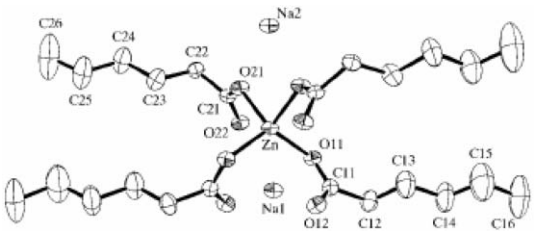

Fig. 6 Structure of $Na_2[Zn(\eta^1\text{-}O_2C_6H_{11})_4]$ (Reproduced from ref. 49 with permission. Copyright 2000, International Union of Crystallography.)

All zirconium centers are six-coordinate. The lead atoms belonging to the BB, are six-coordinate with distorted trigonal prism geometry whereas those who ensure the junctions between the BB *via* a Pb_2O_2 ring, are seven coordinate with a distorted pentagonal bipyramid geometry. The lone pairs on lead appear stereochemically inactive with no obvious vacancy in the first coordination sphere. The structure of $Pb_2Ti_4(\mu\text{-}O_2CR')_4(\mu\text{-}OR)_6(\mu_3\text{-}OR)_2(OR)_8$ (R = Pr^i, R′ = $CHEtC_4H_9$) is also centrosymmetric and based on triangular $Ti_2Pb(O_2CR')(OR)_8$ units.[8] However, the building blocks are

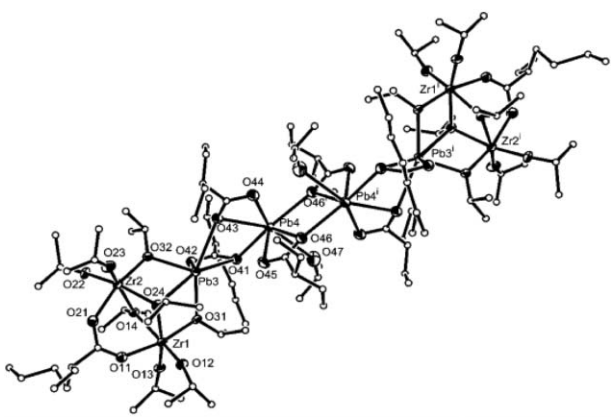

Fig. 7 Structure of $[Pb_4Zr_4(\mu\text{-}O_2CCHEtC_4H_9)_4(\mu\text{-}OPr^i)_6(\mu_3\text{-}OPr^i)_2(OPr^i)_8(Pr^iOH)_2]$ (Reproduced from ref. 8 with permission. Copyright 2006, Royal Society of Chemistry.)

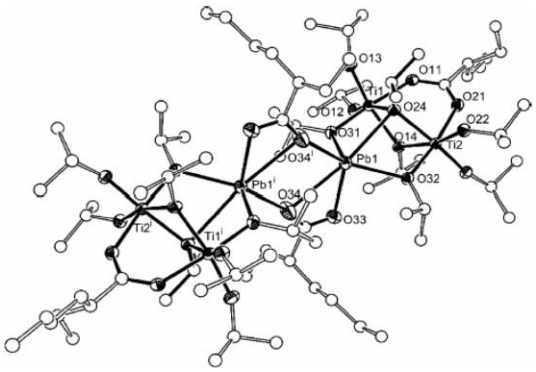

Fig. 8 Structure of $[Pb_2Ti_4(\mu\text{-}O_2CCHEtC_4H_9)_4(\mu\text{-}OPr^i)_6(\mu_3\text{-}OPr^i)_2(OPr^i)_8]$ (Reproduced from ref. 8 with permission. Copyright 2006, Royal Society of Chemistry.)

linked by their lead atoms *via* bridging chelating μ,η^2-2-ethylhexanoate ligands and its overall stoichiometry is thus that of the BB (Fig. 8). This results in a slightly asymmetrical bridge [2.803(6) and 2.909(7) Å] and in six-coordinate lead centers. In contrast with the Pb–M heterometallic species based on acetates,[4–6] the 2-ethylhexanoate ligands display in both of two cases above, two types of coordination modes, bridging and bridging-chelating.

Despite the unusual $M_2M'_3$ stoichiometry, the structure of $Pb_2Ti_3(\mu_4\text{-}O)(\mu_3\text{-}O)(\mu\text{-}O_2CC_7H_{15})_2(\mu\text{-}OPr^i)_6(OPr^i)_4$ is quite symmetrical (Fig. 9) and can be seen as a $Pb_2Ti_2O_2(\mu\text{-}O_2CR')_2(OR)_6$ species having two types of oxo ligands namely a central μ_4-O2 and a peripheral O1 which acts as ligand toward a $Ti(OPr^i)_4$ moiety leading to a five-coordinate titanium centre.[8] This μ_3-oxo ligand O1 has a quite regular planar trigonal geometry. In contrast, the stereochemistry of the tetragonal oxo ligand is distorted with an increase in the Ti2···Ti2′ distance up to 3.608 Å, as well as an opening of the Ti2O2Ti2′ angle [up to 136.2(4)°] for accommodation of the two bridging alkanoates. In contrast with $Pb_4Zr_4(\mu\text{-}O_2CCHEtC_4H_9)_4(\mu\text{-}OPr^i)_6(\mu_3\text{-}OPr^i)_2(OPr^i)_8(Pr^iOH)_2$ and $Pb_2Ti_4(\mu\text{-}O_2CCHEtC_4H_9)_4(\mu\text{-}OPr^i)_6(\mu_3\text{-}OPr^i)_2(OPr^i)_8$, the lone pairs of the five-coordinate tetragonal pyramidal lead centers are stereochemically active.

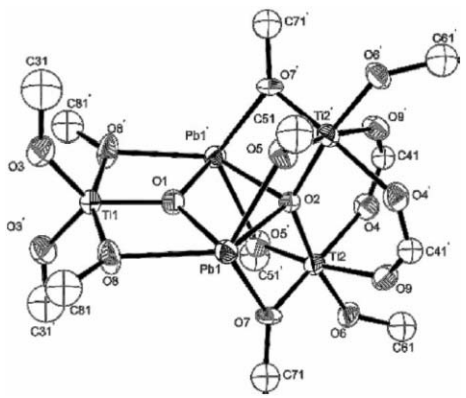

Fig. 9 Structure of $[Pb_2Ti_3(\mu_4\text{-}O)(\mu_3\text{-}O)(\mu\text{-}O_2CC_7H_{15})_2(\mu\text{-}OPr^i)_6(OPr^i)_4]$, disordered C atoms are omitted for clarity (Reproduced from ref. 8 with permission. Copyright 2006, Royal Society of Chemistry.)

3.2 Spectroscopic characterization

Among the various spectroscopic methods employed for identification and characterization of metal alkanoates, FT-IR is the most diagnostic.[54] Their IR spectra are dominated by strong absorptions in the carbonyl region. The antisymmetric stretching vibrations, $\nu_{as}(CO_2)$, appear between 1640 and 1600 cm^{-1}, whereas corresponding symmetric stretches, $\nu_s(CO_2)$, are observed between 1440 and 1380 cm^{-1}. For metal alkanoates, these bands are shifted to lower frequencies compared to those of the free alkanoic acid. The frequency difference between the antisymmetric and symmetric stretches [$\Delta\nu = \nu_{as}(CO_2) - \nu_s(CO_2)$] has been used to distinguish the types of bonding of alkanoate ligands. The $\Delta\nu$ value decreases in the order unidentate > ionic > bridging > bidentate.[54] Raman spectroscopy too sheds light on different structural aspects such as lateral chain packing of alkanoate moieties and metal–metal interaction in $M_2(O_2CR)_4$ types of compounds.[44] It has also been used as a sensitive probe to study the mesomorphic behaviour. For example, the rhodium-rhodium stretching mode at 340–350 cm^{-1} in the Raman spectra of $Rh_2(O_2CR)_4$ (R = C_5H_{11}, C_7H_{15}),[44] shifts continuously to lower values while its half-width increases on heating. The lowering of wavenumbers indicates weakening of Rh–Rh bond, whereas broadening results from the stronger disorder of the alkyl chains in the liquid crystalline phase.[44]

^1H and ^{13}C NMR studies have been carried out on metal alkanoate derivatives of diamagnetic metals to seek structural informations and also to study their mesophases.[8,9,33,37,43,46,51] For example, the ^1H NMR spectrum of homometallic, heteroleptic $[Ti(OC_4H_9)_2(O_2CCHEtC_4H_9)_2]$ shows two groups of peaks at 3.72 and 4.14 ppm due to the methylene protons alpha to the oxygen atoms, indicating the presence of both *cis* and *trans* isomers in the solution.[46] Bardet *et al.*[43] measured the ^{13}C NMR spectra of $Rh_2(O_2CC_4H_9)_4$ and $Rh_2(O_2CC_8H_{17})_4$ and compared them with a X-ray crystallographically characterized compound, $Rh_2(O_2CC_3H_7)_4$. The large shift (*ca.* 20 ppm) of alkanoate resonance to higher frequency relative to the corresponding isotropic resonance (170–176 ppm) of silver alkanoates was explained by the deshielding effect of the Rh–Rh single bond. Furthermore, the splitting of resonances of the alkanoate (C-1) and the terminal methyl (C-5 and C-9, respectively) carbon atoms as well as that of C-3 were explained by assuming that $Rh_2(O_2CR)_4$ (R = C_4H_9, C_8H_{17}) have paddle-wheel type of structure with weak intermolecular Rh···O bonds. To provide insights into metal coordination chemistry, ^{95}Mo, ^{119}Sn and ^{207}Pb NMR studies have also been used for characterisation of alkanoates of these metals.[8,9,33,55]

The EPR spectra of three structurally different copper(II) hexanoates namely dinuclear $[Cu_2(O_2CC_5H_{11})_4(urea)_2]$, tetranuclear $[Cu_2(O_2CC_5H_{11})_4(urea)]_2$, and polynuclear $[Cu_2(O_2CC_5H_{11})_4]_\infty$ showed comparable features, which could be explained on assuming tetranuclear species as hybrid example of both dinuclear and polynuclear species.[23] A classical copper acetate hydrate type of three resonance lines (H_{z1}, $H_\perp$ and H_{z2}) were observed in the rt EPR spectrum of dinuclear $[Cu_2(O_2CC_5H_{11})_4(urea)_2]$, whereas the polymeric $[Cu_2(O_2CC_5H_{11})_4]_\infty$ showed broad and poorly resolved bands with strongest signal being positioned between 300 and 430 mT. By lowering the temperature to the 95 K, H_{z1} signal in the spectrum of $[Cu_2(O_2CC_5H_{11})_4(urea)_2]$ split, due to hyperfine interaction of the unpaired electron with two equivalent copper nuclei within the dinuclear unit (A = 6.2 mT), whereas the dominant signal between 300 and 430 mT in the spectrum of $[Cu_2(O_2CC_5H_{11})_4]_\infty$ disappeared. On the other hand, in the rt EPR spectrum of tetranuclear $[Cu_2(O_2CC_5H_{11})_4(urea)]_2$, several additional signals were observed besides three characteristic triplet signals. The regions of these signals, their disappearance from the spectra by lowering of the temperature to 95 K and the simultaneously narrowing of the three copper acetate hydrate type signals, was in close correlation with the observations for the polynuclear $[Cu_2(O_2CC_5H_{11})_4]_\infty$. The origins of these additional signals were explained by the Cu–O inter-dinuclear interactions.[23]

The UV-Vis spectroscopic studies of alkanoates of copper[18] and lanthanides[25] have also been carried out. These spectra show broad and asymmetric d-d transitions in the region 670–700 nm for polymeric copper(II) alkanoates (*i.e.* without any Lewis base), suggesting an octahedral geometry with considerable tetragonal distortion around the metal. A weaker band is also found at around 375 nm, which is associated with a binuclear Cu(II) alkanoates configuration.[18] In addition, ligand-to-metal charge transfer (LMCT) bands are also observed in the case of Lewis base adducts of copper(II) alkanoates.[18]

The ESI mass spectrometry studies of commercially available 2-ethylhexanoates of iron, cobalt, manganese and tin show that they are complex mixtures of several metal ion clusters of different sizes.[34,55] The μ_3-oxo bridged trinuclear iron(III) cluster structure is confirmed by a peak at m/z = 1042.6 in the ESI-MS spectrum of $[Fe^{III}_3(\mu_3\text{-}O)(O_2CCHEtC_4H_9)_6]^+$ in isopropanol ($HOPr^i$).[34] The ESI mass spectrum of structurally characterized[24] mixed-valent manganese compound, $[Mn^{II}_2Mn^{III}_2(\mu_3\text{-}O)_2(2\text{-ethylhexanoate})_6(bpy)_2]$ contains four different series of peaks.[34]

The ^{119}Sn Mössbauer spectrum of commercially available Sn(II) 2-ethylhexanoate shows two quadrupole-split spectral doublets readily assignable to two oxidation states, *i.e.*, Sn(II) and Sn(IV).[55] The ^{57}Fe Mössbauer spectra of $[Fe^{III}_3(\mu_3\text{-}O)(O_2CCHEtC_4H_9)_6]^+$ clearly reveal the presence of two slightly different iron(III) sites.[56] The area ratio of the two spectral components was very close to 1 : 2 at all temperatures as would be expected if $[Fe^{III}_3(\mu_3\text{-}O)(O_2CCHEtC_4H_9)_6]^+$ adopts an isosceles rather than an equilateral triangular geometry. As expected, the isomer shifts (δ) of the two iron(III) sites are similar and are typical of iron(III) in a basic trinuclear μ-oxo iron(III) complex such as $[Fe_3O(O_2CH)_6(H_2O)_3]^+$ and $[Fe_3O(O_2CCH_3)_6(H_2O)_3]^+$.[50] In contrast, the quadrupole splittings, ΔEQ, are rather different for the two sites and indicate that the unique iron(III) site has a more distorted electronic environment than do the two equivalent iron(III) sites.

3.3 Magnetism

Mononuclear copper(II) alkanoate complexes have essentially temperature-dependent magnetic moments, in the range of

1.75–2.20 μ_B[16,17,20–22] indicating interactions between unpaired electrons. On the other hand, di- and polynuclear copper(II) complexes have magnetic moments smaller than these values due to the antiferromagnetic coupling *via* the alkanoate groups. For example, the anhydrous copper(II) hexanoate exhibits a μ_{eff} value of 2.10 μ_B at 290 K indicating that the system is weakly coupled.[36] As expected for the ground state of an antiferromagnetically coupled dinuclear copper(II) complex, by lowering the temperature from 290 to 2 K, the μ_{eff} decreases monotonically and approaches a broad minimum of 0.15 μ_B at 2 K.[36] The ruthenium complexes of the type $Ru_2(O_2CR)_4X$ (R = C_5H_{11} to $C_{12}H_{25}$ and higher; X = Cl^-, O_2CR^-) display strong zero-field splittings (D) ranging from 60 to 94 cm^{-1}.[10b,c] The zJ values, found in the range -0.09 to -4.6 cm^{-1}, indicate antiferromagnetic exchange. The magnetic properties of $[Fe_3O(O_2CC_6H_{13})_6(H_2O)_3]NO_3$[32] and $[Fe_3O(O_2CCHEtC_4H_9)_6(acetone)_3](HO_2CCHEtC_4H_9)$[56] have been studied in detail. The two possible exchange pathways possible for these complexes are (i) the central oxygen atom and (ii) the bridging alkanoate anions. The antiferromagnetic interaction in these complexes arises primarily within the Fe_3O unit. From the magnetic point of view, these compounds can be viewed as an assembly of quasi-isolated triangular units of Fe(III) ions with S = 5/2 spins where each exchange pathway involves one alkanoate bridge and the central oxygen atom OC(1) or OC(2).[32,56]

4 Physico-chemical properties

In general metal alkanoates, either solids or liquids of different viscosity, are largely air-stable and mostly soluble in common organic solvents. Only few derivatives such as 2-ethylhexanoates of Mn(II)[24] and Ce(III)[57] are exceptionally air- and/or light-sensitive. The coordinatively unsaturated metal alkanoates behave as Lewis acids and either form molecular adducts with a Lewis base (water,[16,17,24,32] alcohols,[57] N-donor ligands)[14,16,22,24,30,31] or oligomerize by intermolecular association.[13,15,36,40] The presence of water molecules in the coordination sphere of large number of metal alkanoates[16,17,24,32] shows that they are hydrolytically stable. However, 2-ethylhexanoates of Sn(II) and Fe(III) have been shown to undergo slow hydrolysis on ageing.[55,56] The ageing has also been shown to decrease the viscosity of Ce(III) 2-ethylhexanoate.[57] The IR and other studies suggests a transformation of Ce(III) to Ce(IV), leading to a smaller metallic ion and thus a less extent of polymerization, as possible explanation for this decrease in viscosity.

Thermal and mesomorphic properties are the most important properties of metal alkanoates, which have played an important role in the evaluation of a significant interest on the study of liquid-crystalline properties of coordination compounds. TGA studies of metal 2-ethylhexanoates show either a two-[58] or a three-stages[57] decomposition process. For Bi(III) 2-ethylhexanoate, experiments in flowing N_2 show that 2-ethylhexanoate ligand itself serves as the oxygen source in forming the bismuth oxide.[58] By using pure H_2, pure bismuth is formed rather than β-Bi_2O_3.[58] The mesomorphism of alkanoate derivatives of the metals such as Mo,[33,59] Cu,[60] Ru,[41,42,52] Rh[61] and Ln[25,26] has been extensively studied. The different thermotropic behaviour of metal alkanoates $M_2(O_2CR)_4$ (M = Cr, Mo, W, Cu, Rh, Ru) and the mixed-valent ruthenium(II/III) complexes of the type $Ru_2(O_2CR)_4X$, (where X = Cl^-, $CH_3(CH_2)_{n-2}CO_2^-$ and dodecyl sulfate) can be traced to (i) the relative strength of the M···O intermolecular interactions between $M_2(O_2CR)_4$ units that are preserved in the mesophase, and (ii) varying effects of alkyl group R and counterion X^-.[33,52] Mesomorphic properties of mixtures of metal (same or different) alkanoates have also been studied[59,61] in view of the fact that almost all applications in liquid crystal technology employ mixtures and not the single metal complex. However, due to the space limitation and also the fact that applications in material sciences is the main theme of this article, further discussions on mesomorphism are omitted. Some excellent review articles are available on the subject matter for readers interested in detailed study.[62]

5 Applications

5.1 In materials science

As mentioned in the introduction, metal 2-ethylhexanoates are choice precursors to obtain nano-films, -composites, and –particles by CSD methods such as MOD, PMOD or sol–gel. The medium sized carbon chain is long enough to lower the intermolecular interactions, allowing the formation of high-quality thin (50–1000 nm) films by spin coating onto a suitable substrate but, at the same time, does not have too much organics to eliminate, and thus minimize the size of the pores and other defects in the film. They also provide a mixture with sufficient viscosity—a property that minimizes the cation segregation.[39] Another advantage is plasticity of the film. Unlike alkoxide precursors, which often afford 'mud cracked' because gels are usually brittle, more plasticity is offered by metal 2-ethylhexanoates.[57] The shelf-life of sol (precipitate-free sol) obtained from metal 2-ethylhexanoate is usually longer, which is important for the industrial applications. Medium sized metal alkanoates are also preferred for photochemical metal organic deposition (PMOD) due to their excellent photo-activity. Moreover, they are inexpensive, air-stable, non-toxic as well as commercially available for a wide number of elements.

5.1.1 Nano-films and composites.

(a) Metal organic deposition (MOD). Metal organic deposition (MOD) is one of the popular chemical solution deposition (CSD) methods in which coating of an organic precursor solution on a substrate is followed by thermal decomposition to form the final desired materials. Main advantages of MOD are: (i) low cost, as the use of high vacuum apparatus is not necessary, (ii) precise control of the composition, and (iii) easiness of formation of a large film. Several reports have described the use of metal 2-ethylhexanoates for MOD, which are described below briefly.

(i) Metallic nanofilms. Nanoporous bismuth films were obtained by spin coating a solution of Bi(III) 2-ethylhexanoate and 5% glycerol in isopropanol with subsequent heat treatment in hydrogen environment between 250–270 °C.[58] The porosity

of the resulting films varied from 30 to 50% and pores were present in the form of nano-dimensional channels (5–10 nm wide) existing between bismuth grains of av. 30 nm size. Hydrogen plasma etching was necessitated to lower the residual carbon contents in the films and to remove some oxide impurity (β-Bi_2O_3). The use of this precursor offers (i) a microstructure of Bi films of the type, which is desired for increasing the transport properties of thermo-electric materials, and (ii) almost complete conversion to metallic bismuth at temperature 250 °C in H_2 in 1 h (mp of bismuth 271 °C). Films heated for 3 h exhibited an orientation in which the (012) plane was parallel to the bismuth film surface. After 6 h, a trigonal orientation, which is common for bismuth films, was evident.[58]

(ii) Mono-metallic oxide nanofilms. Aluminium oxide thin films of up to 800 nm thickness were prepared by CVD using aluminium(III) 2-ethylhexanoate at 480–700 °C on glass and silicon (100) substrates.[63] The obtained films were transparent and showed no apparent peeling. The above reaction temperature and deposition rates are comparable to the corresponding values for other commonly used precursors such as $AlMe_3$–O_2 (350–500 °C), $Al(OPr^i)_3$ (420–600 °C) and Al(β-diketonate)$_3$ (420 °C).[63] Moreover, the air-stability of Al(III) 2-ethylhexanoate offers an additional advantage over other precursors.

CeO_2 is one of the preferred buffer layers for the fabrication of coated conductors, especially for YBCO processing. Ce(III) 2-ethylhexanoate offers good properties in terms of deposition (desired viscosity, stability of the solution) and transformation into oxide at relatively low temperature.[57,64] Using this precursor, thin ceria (CeO_2) films have been deposited on single crystals and (100) oriented nickel substrates (Ni RABiTs) by spin-coating MOD,[57a] spray MOD technique[57b] or combustion chemical vapor deposition.[64] Unlike CVD technique, it was possible to avoid the oxidation of the metallic substrate by pyrolysing the precursor solution in reducing atmosphere since there is enough oxygen atoms in the precursor to form the oxide. The CeO_2 is formed preferentially to NiO owing to its low Gibbs free energy formation. Moreover, the (200) orientation of the CeO_2 layer was adequate for further growth of HTcS films on top of it. CeO_2 films obtained by combustion chemical vapor deposition showed two types of morphologies.[64] Those produced with the smallest aerosols and at low precursor concentrations resulted in apparently dense material that nucleated and grew on the substrate, whereas larger aerosols and/or higher precursor concentrations resulted in films containing polycrystalline particles, or clusters, in the film and a decreased growth rate of dense material.

α-Fe_2O_3 films consisting of densely packed epitaxial α-Fe_2O_3 particles with a rectangular shape were obtained when iron(III) 2-ethylhexanoate solution in toluene was spin-coated onto an α-Al_2O_3 (012) substrate rinsed with methanol, and subsequently annealed at 800 °C in air.[65] On rinsing α-Al_2O_3 substrate with other solvents such as toluene, *tert*-butanol, *n*-hexanol, hexane, acetic acid and 2-ethylhexanoic acid, round-shaped particles were formed. It was proposed that presence of thin layers of methanol molecules promoted the ordered absorption of iron(III) 2-ethylhexanoate molecules on the substrate and that this ordered state was maintained during elimination of the organic part of the precursor and subsequent high-temperature heat treatment.[65] Nickel oxide films are known to be applicable for magnetoresistance sensors, electro-chromic devices, transparent conducting films, and chemical sensors. The pyrolysis of spin-coated nickel(II) 2-ethylhexanoate films on substrates such as SnO_2-coated glass and Corning 7059 glass at 380 °C in air produced electrochromic NiO films consisted of cubic (200) NiO crystallites of 10–20 nm in diameter.[66] Unlike electrodeposition, the above method allows the deposition of films even on electronic insulating substrates. Moreover, these spin-coated films showed better electrochromic properties than electrodeposited films or those prepared by sol–gel methods.[66] Two-dimensional nanohoneycombs of NiO has also been prepared by solution-based nanosphere lithography (s-NSL) technique using Ni(II) 2-ethylhexanoate, which showed excellent field emission properties.[67]

(iii) Bimetallic oxide nanofilms and composites. Indium tin oxide (ITO) thin films are widely utilized as an essential part of many opto-electronic devices because of their unique properties of high electrical conductivity and high optical transparencies in the visible region. In a unique study of mixing the sol–gel and MOD processes recently, ITO films with molar compositions ranging from 98% In_2O_3–2% SnO_2 to 2% In_2O_3–98% SnO_2 were deposited on silicon substrates by mixing solutions of Sn(II) 2-ethylhexanoate in butanol with In_2O_3 sols prepared by a chemical complexation-based sol–gel process.[68] It was concluded that the main factor governing the film formation is the lack of cross-linking reactions between the tin and indium species in the starting solutions, which may result in phase separation already during the spinning stage. Upon heat treatment up to 800 °C, a peculiar structure formed in the film with 30% In_2O_3, constituted by a mixture of nanocrystals of SnO_2, In_2O_3, and a mixed phase, as confirmed by XRD patterns, EELS spectra and HRTEM images (Fig. 10).

The Au–Co_3O_4 composite film is among the few examples of solid-state gas sensor materials, which can be used for the recognition of CO and H_2 molecules through optical absorbance changes. The gold–cobalt oxide (Au–Co_3O_4) composite films, prepared by the sputter-deposition of gold onto a glass plate substrate followed by pyrolysis of spin-coated cobalt 2-ethylhexanoate, comprised small Au particles and Co_3O_4 nanocrystals.[69] It could optically recognize CO and H_2 in air over a wide range of concentration. The Vis–Near IR plasmon absorption band near 600 nm of small Au particles was not changed by CO but was selectively increased by H_2. Outside the plasmon band, near 900 nm, both CO and H_2 reduced the light absorption ability of the Co_3O_4 moiety in the film. Therefore, absorption measurements at both 600 and 900 nm made it possible to distinguish H_2 from CO in air.

Lanthanum nickel oxide (LNO) has low resistivity and is isotropic in nature, and therefore, is a promising candidate for an electrode. Conductive LNO films were grown on various substrates such as STO, fused quartz, and Si using 2-ethylhexanoates of lanthanum and nickel.[70] The results on effect of different thermal treatments, annealing temperature and substrates on crystallinity, orientation and conductive

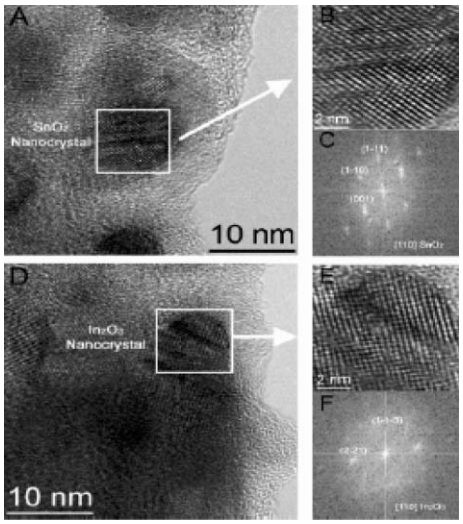

Fig. 10 HRTEM images of the different regions of ITO films with 30% In_2O_3-70% SnO_2 composition, heated at 800 °C (A and D), showing the co-existance of SnO_2 nanocrystals (B and, in C, the related power spectra (FFT)), and of In_2O_3 nanocrystals (E and, in F, the related power spectra (FFT)) (Reproduced from ref. 68 with permission. Copyright 2006, American Chemical Society.)

behaviour of these films indicated that pyrolysis process is the critical step to obtain good metallic LNO films at lower temperature. Epitaxial metallic LNO films could be fabricated on STO due to the matched perovskite structure between LNO and STO. The trend of resistance as a function of annealing temperature of LNO films on different substrates showed LNO films on STO have lower crystallinity temperature and higher transition temperature from conductor to insulator than on fused quartz and Si.

Yttria-stabilized zirconia (YSZ) is a widely used ceramic because of its high toughness, high bending strength and low thermal conductivity. Thick and uniform YSZ films with columnar growth features have reportedly been deposited using zirconium(IV) butoxide and yttrium(III) 2-ethylhexanoate in butanol and characterized by SEM, XRD and Raman spectroscopy.[71] The XRD data showed the presence of both tetragonal and cubic phases, the former one being the major phase. The crystallite size of the YSZ in the as-deposited condition was found to be 4 nm, which increased by 10-fold after heat-treatment, owing to grain growth.[71]

Barium- and/or lead-based perovskite mixed-metal oxides have attracted much attention for their applications in a variety of microelectronic. Barium- and/or lead-based bimetallic oxide ferroelectric thin films such as $BaTiO_3$ (BTO),[72] $BaZrO_3$ (BZO)[73] and $BaPbO_3$[74] have been prepared using metal 2-ethylhexanoates as starting materials. BTO and STO ($SrTiO_3$) films were prepared by spin coating on p-type single crystal Si (100) wafers, stainless steel and fused silica using M(II) 2-ethylhexanoate (M = Ba, Sr) and Ti(IV) *n*-butoxide[72] and annealed to give polycrystalline, transparent and crack-free films. Crystalline phases could form at an annealing temperature of 450 °C for STO and 550 °C and above for BTO.[72] SEM images of these films annealed at 700 °C on silicon substrate revealed dense microstructure with uniform thickness and without any microcracks.

(iv) Tri- and multi-metallic oxide nanofilms. Barium- and/or lead-based trimetallic oxide ferroelectric thin films such as BST,[45,75] $Ba(Pb_{1-x}Bi_x)O_3$[74] and PZT[76,77] have also been prepared using metal 2-ethylhexanoates as starting materials. A simple system consisting of 2-ethylhexanoates of Ba(II) and Sr(II) as well as $Ti(OPr^i)_2\{(OC_2H_4)_2NH\}$ in isopropanol has recently been reported for the preparation of stable precursor solutions for dip coating BST thin films.[45] From such stable solutions highly crystalline, uniform and crack-free thin films were obtained by dip coating, followed by annealing at temperatures as low as 600 °C due to crystallization of the perovskite phase through an intermediate-free pathway. Cross-sectional SEM images (Fig. 11) indicated a well-densified structure with some columnar grains. Grain growth across the film thickness is because of the high density of the film and the thickness of a single layer corresponding almost to the grain diameter (60 nm). The dielectric characteristics of the thin films indicated their suitability for applications in tunable devices. Highly (111) oriented PZT thin films, with an excellent combination of electrical properties, were deposited on platinised substrates using 2-ethylhexanoate derivatives of component metals.[76,77] Significant lead volatilization occurred during furnace annealing and high Pb excesses, usually 10–30%, in starting solutions were required to compensate for this. In one case, PZT films exhibited large rosette structures with grain sizes of several microns.[76] It was concluded that the formation of rosette structure could be suppressed by baking coated films in an inert atmosphere.

Recently, bismuth-based perovskite ferroelectric thin films such as SBT and SBN have been candidates for non-volatile ferroelectric memory (NVFRAM) applications. The stability and formation of pyrochlore phase in SBT films prepared by metal 2-ethylhexanoate precursors on $Pt/Ti/SiO_2/Si$ substrates and effect of the doping cations on pyrochlore phase formation and microstructure evolution were studied.[78–80] The pyrochlore phase formation has been identified due to out-diffusion of titanium from underneath platinum layer to participate in the reaction with the films. A model based on the binding energy of octahedral structure was used to elucidate the formation and stability of the pyrochlore phase present in the SBT film. The substitution of both tungsten and vanadium

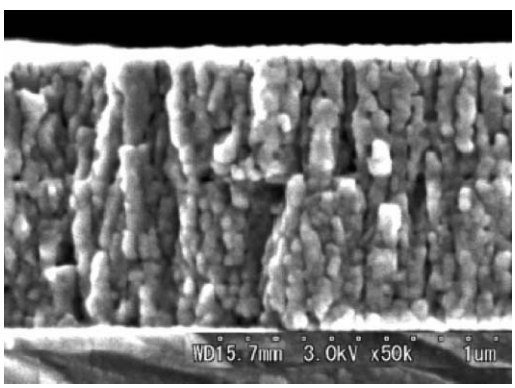

Fig. 11 SEM image of cross-section of BST thin film on a glass substrate indicating a structure with some columnar grains (Reproduced from ref. 45 with permission. Copyright 2006, Blackwell Publishing.)

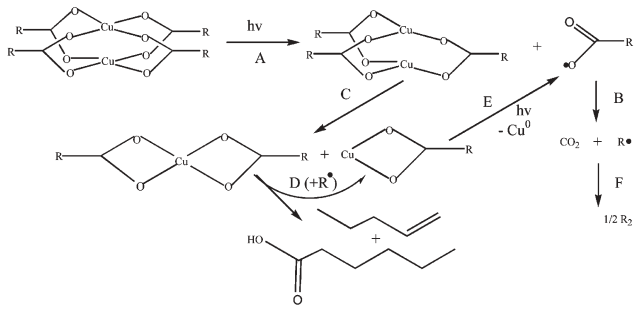

Scheme 4 Mechanism of the photodeposition of copper by photolysis of thin films of $Cu_2(OH_2)_2(O_2CC_5H_{11})_4$.

for tantalum led to the formation of pyrochlore phase at lower annealing temperature (750–800 °C). On the other hand, the addition of zirconium retarded the formation of pyrochlore phase from 850 to 900 °C.[79]

(b) Photochemical metal organic deposition (PMOD). The PMOD method consists of deposition of an amorphous film of a metal alkanoate precursor, followed by its photochemical decomposition into the materials of interest *i.e.* metal or metal oxide. Since the photolytic step in PMOD is normally conducted at rt, the film is usually amorphous. The photodeposition of Cu^0 or Cu_2O, depending upon the conditions of photolysis of thin films of $Cu_2(OH_2)_2(O_2CC_5H_{11})_4$, was first demonstrated by Hill *et al.*[81] Irradiation under a flow of H_2 produced copper films of highest purity. A mechanism based on mass spectral characterization of carbon dioxide, 1-pentene, hexanoic acid, and decane as organic products released during photochemical reaction and also the known chemistry of copper carboxylates was proposed by the authors (Scheme 4). Further sulfidization of these copper thin films deposited on ITO substrate gave Cu_xS (where x is close to 2) thin films, which find application in the Cu_2S/CdS solar cells.[82] AFM images of deposits of copper (and also some cuprous oxides) and Cu_xS on ITO showed that they are preferentially located in the valleys delimited by ITO particles (Fig. 12). The average particle size found was close to 65 and 62 nm for Cu and Cu_xS, respectively. A number of other metal 2-ethylhexanoate derivatives such as those of cerium,[83] lead,[84] titanium,[46] manganese,[85] nickel,[86] and molybdenum[87] have also been used as precursors for PMOD. In most cases the photoreaction is

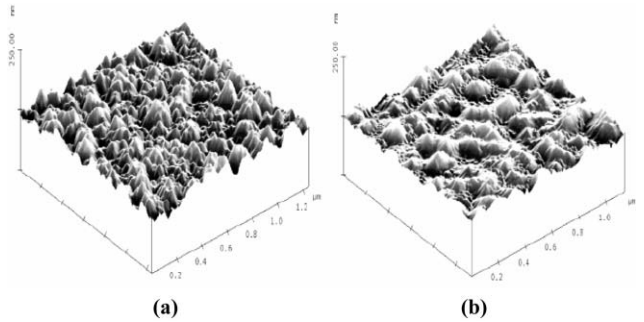

Fig. 12 AFM images of (a) ITO/Cu and (b) ITO/Cu_xS (Reproduced from ref. 82 with permission. Copyright 2002, American Chemical Society.)

believed to involve a ligand to metal charge transfer (LMCT) excited state. The reactions proceed by loss of the alkanoate ligand from the film in the form of carbon dioxide, heptane and heptene (through the intermediacy of the heptyl radical). The photoproduced films are amorphous in most of the cases and crystallized films could be obtained after annealing at 200–500 °C. Multimetallic oxides such as PZT[87–89] and $Bi_2Sr_2CaCu_2O_{8+x}$[89] have also been prepared by PMOD using 2-ethylhexanoate precursors. PZT film was successfully self-patterned without using photoresist and dry etching procedure.[88] Self-patterning of the film could be accomplished after UV exposure and removal of unexposed area of the film by rinsing with hexane. The crystallization of PZT film on Pt (111) substrate showed highly (111) preferred orientational growth of the film. PZT film with perovskite structure gave a well-developed *P–E* hysteresis behavior but slightly shifted to a negative bias direction.[88]

(c) Sol–Gel method. The sol–gel process is based on the hydrolysis and condensation of molecular precursors and offers a lower processing temperature, lower cost and ease of fabrication of large area films. Sol–gel derived pure SnO_2 thin films as well as films doped with platinum and antimony have been prepared from the tin(II) 2-ethylhexanoate and characterized by AFM, RBS and SEM techniques.[90] The sol obtained above from tin(II) 2-ethylhexanoate and doped with 1–2% antimony or platinum has a shelf-life longer than seven days, which is important for the industrial applications. These films deposited on porous silicon substrates were able to fill the pores of porous silicon by using a surfactant agent.[90] Perovskite lead zirconate, $PbZrO_3$ (PZ) has been obtained by sol–gel process using a single-source precursor (SSP), $Pb_4Zr_4(O_2CCHEtC_4H_9)_8(OPr^i)_{16}(HOPr^i)_2$[8,9] at a temperature which is lower than that of using mixtures of lead and zirconium compounds. The TGA and DTA patterns of the products obtained by hydrolysis of this SSP with an excess of water (hydrolysis ratio = 70) in isopropanol showed several strong exothermic peaks in the range 250–450 °C corresponding to the combustion of the remaining organics. The overall weight loss was in agreement with a $PbZrO(O_2CCHEtC_4H_9)$-(Pr^iOH) formula (37 *vs.* 37.8% theoretical). Crystallization of the orthorhombic $PbZrO_3$ structure started after annealing under air around 500 °C, some peaks indexing as pyrochlore were also observed. Annealing at 600 °C was required for a pure perovskite phase. Hydrolysis in forced conditions (refluxing THF, large excess of water) in the presence of tetramethylammonium hydroxide resulted in a higher loss of organics (only about 25% residues by TGA) and to slightly smaller crystallites, but those were agglomerated as shown by SEM photographs.[9]

The $BaCO_3$-free BST thin films were prepared by sol–gel method[91,92] using a sol derived from barium(II) 2-ethylhexanoate, strontium(II) 2-ethylhexanoate and titanium(IV) isopropoxide and modified by acetylacetone/formamide[91] or pyrrole.[92] Epitaxially-grown BST was deposited on Pt/MgO(100) substrate by multi-layered spinning technique and calcined at 650 °C in oxygen for 1 h, the XRD pattern of which showed that (001) planes of BST films were mainly laid parallel to Pt(100) and MgO(100).[91] The thickness of these

crack-free transparent films were 350 nm, which increased by twofold (645 nm) when pyrrole concentration was increased from 0.5 to 1.5 molar ratio with respect to titanium.[92] Crystallisation started at 650 °C and completed at 900 °C. Films of SBT and SBN, two most important ferroelectric oxides for non-volatile memory, have been deposited by the sol–gel method using metal 2-ethylhexanoates.[93,94] The backing sequence chosen for the deposition of SBT films had an important influence on the electrical, morphological and chemical characteristics of the FE. Slow baking that leads to a complete pyrolysis of the metalloorganic film without reduction of the bismuth resulted in a larger grain size. A bismuth-rich layer at the surface of the film and its depletion immediately below was explained in terms of partially reduced bismuth, which diffuses to the film surface during heat treatment.[93] SBN thin films with thickness close to 30 nm were deposited on single crystalline (001) $SrTiO_3$ substrate.[94] XRD studies of it showed that, though crystallization starts at 500 °C, these crystallites do not present the typical 'Aurivillius phase' before 600 °C. The weak intensities of the diffraction lines and their decrease when the sample is annealed above 600 °C showed that the number of disoriented grains was quite low and decreased with further annealing.

5.1.2 Nanoparticles. Several reports on successful processing of metal 2-ethylhexanoates *via* sol–gel, MOD, flame spray pyrolysis or ultrasonication methods for obtaining highly crystalline metal oxide or non-oxide (sulfide, telluride, halides) nanoparticles have been published.[39,94–107] These results are described briefly below.

(a) Metal nanoparticles. Stable silver nanoparticles (av. diameter 4.4 nm) capped with 2-ethylhexanoate have been prepared by addition of silver 2-ethylhexanoate to dimethyl sulfoxide (DMSO) in the presence of trisodium citrate as a stabilizer.[95] Experimental and theoretical results suggested that the reduction of silver 2-ethylhexanoate takes place through a precursor species, [Ag(DMSO)(2-ethylhexanoate)]. The enlarged width of electronic absorption spectra was explained by the defects, such as stacking faults and twinning, as well as by citrate species interacting at nanoparticles surface. UV-Vis spectra showed that these silver nanoparticles in DMSO react with NO, thus causing the dissolution of metal.[95] Highly air stable, face-centered-cubic cobalt nanoparticles were prepared by a modified flame spray pyrolysis (FSP) method[96] in which the use of fuel rich flames and a sinter-metal tube for enhanced gas mixing during the reaction gave rise to highly reducing conditions favouring the formation of metallic cobalt. These nanoparticles of 20–60 nm diameter were protected against oxidation by a surface layer of less than 1 nm of cobalt oxide.

Intermetallic PtPb nanoparticles have been synthesized by the chemical reduction of dimethyl(1,5-cyclooctadiene)- platinum and lead(II) 2-ethylhexanoate by sodium naphthalide in THF or diglyme.[97] If exposed to air quickly, the product was crystalline PtPb with a mean crystal domain size of 16 nm (as shown by XRD). On exposure to air slowly, the XRD pattern showed much broader and weaker peaks. Performing the synthesis in diglyme allowed the crystal domain size to be controlled by annealing at temperatures below the boiling point of diglyme (162 °C). These PtPb nanoparticles exhibited a remarkable ability to oxidize formic acid, with high mass activities and onset potentials similar to those reported previously for bulk PtPb electrodes.[97]

(b) Metallic oxide nanoparticles. Using the sol–gel method, nanocrystalline zinc oxide powders were prepared by fast hydrolysis of Zn(II) 2-ethylhexanoate in isopropanol, adding tetramethylammonium (TMAH) aqueous solution.[98,99] TEM and XRD studies showed that particle and crystallite sizes in ZnO powders were approximately equal. Cylinder (prism)-shaped crystallites had shorter base diameter (25–35 nm) than the height (35–45 nm), whereas size of ZnO particles varied between 20 to 50 nm. Recently, MOD synthesis of soluble ZnO nanocrystals has also been reported by the decomposition of Zinc(II) 2-ethylhexnoate at 250 °C in diphenyl ether.[100] The use of long carbon chain amines as surface capping agents resulted in a 'clean' decomposition of the precursor. The ZnO nanoparticles crystallised in the hexagonal (zincite) phase with size ranging from 5 to 8 nm. The PL curve of ZnO displayed two peaks at about 400 and 560 nm, attributed to the band-edge recombination and emission mediated by oxygen vacancies or other defects, respectively.[100] The band at 560 nm was found much weaker than that at 400 nm, possibly because of the stoichiometric excess of oxygen in the zinc(II) 2-ethylhexanoate precursors (two oxygen atoms for a ZnO stoichiometry), which would limit the oxygen vacancies.

MOD synthesis of soluble SnO_2 nanocrystals has also been reported by the decomposition of Sn(II) 2-ethylhexanoate at 230–250 °C in diphenyl ether and in the presence of amines.[100] The tetragonal SnO_2 crystallised in the cassiterite phase with a mean size ranging from about 3 to 3.5 nm, depending upon the length of the amine chain. Optical properties for SnO_2 nanoparticles were characterized by only a blue luminescence. The OA and PL curves of SnO_2, observed at around 350 and 400 nm and attributed to excitation formation and band-edge emission, respectively, are similar to those of ZnO. However, unlike in ZnO, no emission at around 560 nm was observed, indicating that oxygen vacancies and other defects were absent. Very recently, monodispersed 2.4 nm-sized SnO_2 nanoparticles of the pure cassiterite structure have been reproducibly formed by a non-hydrolytic solvothermal reaction using the same precursor tin(II) 2-ethylhexnoate but without the addition of extra surfactants.[101] During the synthesis, the dissociated 2-ethylhexanoates from the tin metal worked as a capping agent, and this induced size control of the nanoparticles and the suppression of interparticular aggregation. The as-prepared nanoparticles were soluble in nonpolar solvents, and by converting the capping group to a citrate, they also formed transparent suspensions in an aqueous solution.[101] In a previous report, the effect of addition of 2–5% Mo on SnO_2, prepared as regular shaped and nanosized particles from tin(II) 2-ethylhexanoate *via* sol–gel method, was studied in view of their potential applications in gas sensor.[102] SnO_2 doped with Mo were more transparent than pure SnO_2 powders. FTIR showed that Mo lowers the intensity of the light scattered by free electrons, whereas electrical measurements showed that Mo markedly lowers the response of tin

oxide towards CO, but leaves almost unaltered or enhances its ability to sense NO_2, depending on the thermal parameters.[102]

A facile, one-pot sonochemical process has been described for the preparation of γ-alumina nanoparticles using aluminium hydroxyl bis(2-ethylhexanoate) precursor in *n*-decane.[103] The gel formed during this sonication process, has been shown to have polyalumoxane network in which aluminium centres are six-coordinated (^{27}Al NMR evidence). Calcination at 900 °C for 5 h yielded pure γ-Al_2O_3 nanoparticles with size less than 10 nm. Solid-state ^{27}Al NMR spectrum showed that aluminium centres in these nanoparticles are in four- and six-coordination environments.[103] Yttria doped with 5% Eu^{3+} ions nanophosphorparticles (30 nm), Y_2O_3:Eu^{3+} were prepared by FSP using a toluene solution of 2-ethylhexanoate precursors.[104] The crystal size and shape could be closely controlled from monoclinic to cubic by selecting the FSP-process parameters that determine the high temperature particles residence time. Thus, a relatively low enthalpy content and short flame resulted in the formation of spherical pure monoclinic particles with an approximate size of 11 nm, whereas a hotter and longer flame gave cubic shaped (rhombohedral) particles of 15–25 nm size. The characteristic PL emission spectrum of the cubic phase (strongest peak at 612 nm) differed strongly from the monoclinic one (strongest peak at 625 nm). These nanosized flame-made particles showed lower PL intensities than a commercial phosphor but prolonged radiative decay. Compacted powders showed higher PL emission intensities and bulk-like emission intensities decay. Ultrasonication of a mixture of aluminium hydroxyl bis(2-ethylhexanoate) and yttrium(III) 2-ethylhexanoate precursors in *n*-decane produced a gel, which after calcination at 900 °C for 5 h, showed phase pure YAG particles, $Y_3Al_5O_{12}$ with no γ-Al_2O_3 phase.[103] The ^{27}Al solid state NMR spectra of this garnet were consistent with six-, five- and four-coordinated aluminium centres, respectively, in it. Most importantly, sonication process allowed the formation of YAG hundreds of degrees below the commonly used temperature of 1400 °C to get phase pure garnet material. The YAG has also been prepared by FSP using Y(III) 2-ethylhexanoate and $Al(OC_2H_4)_3N$.[105]

The MOD method using 2-ethylhexanoates of lithium and cobalt(II) in THF allowed the preparation of $LiCoO_2$, an important p-semiconductor oxide in the lithium ion battery, without phase segregation and at a temperature (700 °C) which is much lower than that required in solid-state reactions (800–1000 °C).[39] The electrochemical characterization showed that $LiCoO_2$ calcined at 700 °C consists of aggregate particles that permit the preparation of composite electrodes with facile lithium diffusion. The BET analysis and cyclic voltammetry technique have suggested that this facile lithium diffusion might be associated with shape and pore distribution in the grains.[39] The heterometallic oxide nanoparticles of so-called Aurivillius family such as $Bi_4Ti_3O_{12}$,[106] $SrBi_4Ti_4O_{15}$,[107] and SBN[94] have also been synthesized using Bi(III) 2-ethylhexanoate and Sr(II) 2-ethylhexanoate as precursors. The crystallisation of SBN particles began between 500 and 550 °C with XRD showing very broad lines assigned to fluorite-like structure. At 600 °C, the "perovskite" Aurivillius phase began to appear and peaks of this phase sharpened and increased to the detriment of those of the fluorite structure at 650 °C. The sample was completely converted to the SBN Aurivillius phase at 700 °C.[94]

(c) Metal halide nanoparticles. FSP process has also been used for the preparation of metal halide nanoparticles.[108] High purity alkaline earth metal fluorides such as CaF_2, SrF_2 and BaF_2 as well as NaCl have recently been produced by mixing corresponding metal 2-ethylhexanoate liquid precursors with hexafluorobenzene/chlorobenzene and spraying the resulting liquid into a methane–oxygen flame.[108] The high affinity of fluorine and chlorine towards alkali and alkaline earth metals promoted the rapid formation of the corresponding salts and suppressed oxide formation. The produced salts consisted of nanoparticles with diameters of 20 nm for CaF_2 to well above 100 nm for NaCl. TEM images of the fluorides showed regular shaped cubic crystallites for BaF_2 and slightly irregular spheroid nanoparticles for SrF_2 and CaF_2 (Fig. 13).

When switching from CaF_2 to SrF_2 or BaF_2 an increase of the primary particle size was observed together with a decrease of the degree of agglomeration. For applications in optical fibre manufacture for UV-Vis and lasing materials, BaF_2 doped with 1% Ho was also synthesized using a precursor containing barium(II) 2-ethylhexanoate and 1% holmium(III) 2-ethylhexanoate and a stoichiometric amount of hexafluorobenzene.[108] Face-centred cubic AgCl nanoparticles of average size 80 nm and capped by [Cu(II) 2-ethylhexanoate]$^+$ cations were prepared by adding copper(II) 2-ethylhexanoate to negative-charged AgCl sol solution.[109] FT-IR, UV-Vis and XPS studies showed that cupric 2-ethylhexanoate was capped on the surface of AgCl nanoparticles by electrostatic force in the form of [Cu(II) 2-ethylhexanoate]$^+$ ions.

(d) Metal sulfide and telluride nanoparticles. In addition to metal halides, nanoparticles of other metal non-oxides such as sulfide and telluride have also been prepared using metal 2-ethylhexanoates as precursors.[110,111] Cubic CdS nanoparticles of average size 220 nm have been synthesized by ultrasonication method from cadmium(II) 2-ethylhexanoate

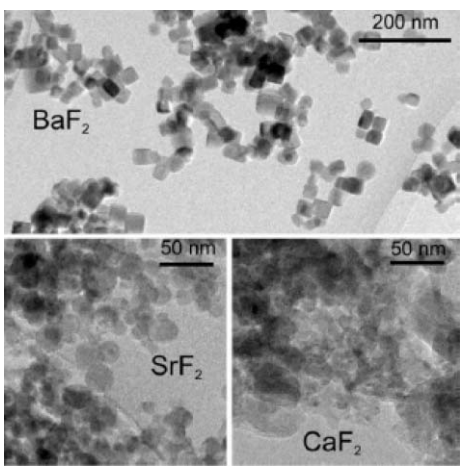

Fig. 13 TEM images of flame-made alkaline earth fluorides (Reproduced from ref. 108 with permission. Copyright 2005, Royal Society of Chemistry.)

and Na_2S in DMSO.[110] The presence of a satellite peak in the XRD of CdS nanoparticles at $2\theta = 28.7^\circ$ was attributed to (101) plane of hexagonally packed CdS due to low activation energy of the cubic-to-hexagonal phase transition. After ripening (3 weeks), CdS nanoparticles displayed a sharp excitonic peak at $\lambda_{max} = 402$ nm, while in freshly prepared dispersions a broad trapped emission at 510 nm dominated. By using one- and two-dimensional NMR spectroscopy, the conformation of the 2-ethylhexanoate ligand adsorbed to the nanoparticles was determined. The observation of two separate triplets corresponding to the terminal methyl groups located on the ethyl and hexyl chains was indicative of a 'wrap-around' conformation, where long hexyl chain of 2-ethylhexanoate ions spreads over the surface of CdS and the short ethyl end is primarily surrounded by DMSO. This packing of the hydrocarbon chains could be perturbed by the surface modification with nucleophiles such as 4,4′-bipyridine, thiophene, trimethylamine and thiomolybdate anions, which resulted in a partial replacement of the 2-ethylhexanoate and reorientation of the hexyl chain away from the surface. The difference in the degree of replacement and/or conformational changes of 2-ethylhexanoate ion depended on the electron donor activity of the modifier.[110]

Bismuth telluride (Bi_2Te_3) is one of the best thermoelectric materials. Synthesis of single-crystal, defect-free, and hexagonal Bi_2Te_3 nanoplatelets has been carried out from Bi(III) 2-ethylhexanoate and Te–TOP (tellurium in trioctylphosphine) as precursors using diphenyl ether and dioctyl ether as solvents and oleic acid as capping agent.[111] The Bi_2Te_3 crystal consists of 15 layers stacked along the *c*-axis and presents the combination of three hexagonal layer stacks of the composition in which each set consists of five atoms (Te_1–Bi–Te_2–Bi–Te_1). The bonding within the Te_1–Bi–Te_2–Bi–Te_1 layer was considered to be covalent, while the bonding between Te_1–Te_1 layers was the van der Waals forces. With the introduction of a small amount of Se–TOP precursor (5% by mol) at 200 °C, these pure Bi_2Te_3 hexagonal nanoplates (Fig. 14) could be epitaxially grown on surface of a Te rod to form strings of platelet structures. In this epitaxial growth, the *c*-direction of Bi_2Te_3 nanoplatelets was parallel to the *c*-axis of the Te rod. A two-step growth process involving formation and fast growth of the Te nanorod along (0001), followed by a nucleation and epitaxial growth of the Bi_2Te_3 nanoplatelets was proposed by the authors.[111] These well-built ID aligned strings formed by 2-ethylhexanoate precursors are desired low-dimensional thermoelectric building-blocks for possibly achieving a high thermoelectric figure of merit.

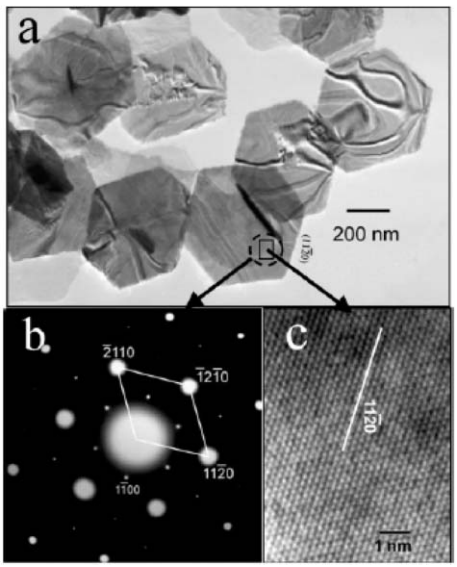

Fig. 14 Bi_2Te_3 nanoplatelets: (a) TEM images, (b) electron diffraction pattern, and (c) HR-TEM image of a selected area (Reproduced from ref. 111 with permission. Copyright 2005, American Chemical Society.)

5.2 Miscellaneous applications

5.2.1 In homogeneous catalysis. Medium sized metal alkanoates, especially 2-ethylhexanoates have been extensively used, either alone or in combination with other complexes, as homogeneous catalysts for a variety of reactions.[112–124] Nickel(II) 2-ethylhexanoate is used as starting material for the preparation of Ziegler nickel catalysts,[112] whereas a 2 : 1 combination of ascorbic acid 6-palmitate and iron(III) 2-ethylhexanoate has been shown to be a very good catalyst for oxidation and oligomerization of ethyl linoleate, a model compound for alkyd resins.[113] Iron(III) 2-ethylhexanoate has also been used as a novel, mild Lewis acid catalyst for the stereoselective Diels–Alder reaction of ethyl (*E*)-4-oxobutanoate with alkyl vinyl ethers (alkyl = ethyl, isobutyl, *n*-butyl) to stereoselectively produce *cis*-2-alkoxy-3,4-dihydro-2*H*-pyran-4-carboxylic acid, ethyl esters with diastereoisomeric excesses (de) in as high as 98% yield.[114]

Importance of choice of metal ligand and metal oxidation state is reflected by the fact that similar catalysts containing lower metal oxidation states and/or ligands, which are bulkier and/or more rigid (naphthenate, benzoate, stearate) give lower selectivity as well as lower reaction yields. Some other applications of metal alkanoates as catalyst are: Bi(III) hexanoate for polyesters of ethane diol and adipic or sebacic acid,[115] Zn(II) 2-ethylhexanoate in ROP[116] and the catalytic activity of Ni(II) 2-ethylhexanoate and Co(II) 2-ethylhexanoate, in combination with methylaluminoxane, in the polymerization of norbornene.[117]

Out of many catalytic applications mentioned above, the role of metal alkanoates as catalysts in ring opening polymerization of lactone and lactides is the most important one[11] and, therefore, is being briefly described below.

(a) Ring opening polymerization of lactones and lactides. Ring opening polymerization (ROP) of lactones and lactides has been thoroughly investigated during the last 40 years, due to its versatility in producing a variety of biomedical polymers in a controlled manner.[118–124] A catalyst or initiator is necessary to start the polymerization at mild conditions and to get high-molecular weight polyesters of low polydispersity in short periods of time. Depending on the initiator (catalysts), the polymerization proceeds according to three different reaction mechanisms, *viz*, cationic, anionic, or coordination-insertion mechanisms.[11] Tin(II) 2-ethylhexanoate is a frequently used catalyst in the ROP of lactones and lactides[118] and is prototype

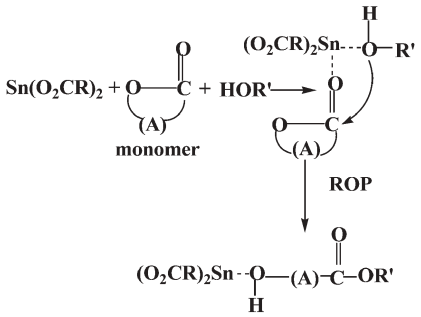

Scheme 5 Coordination–insertion mechanism of ROP by tin(II) 2-ethylhexanoate as proposed by Kricheldorf and co-workers.[120]

of coordination-insertion ROP. The mechanism of ring opening polymerization by tin(II) 2-ethylhexanoate has been widely discussed.[119,120] Tin(II) 2-ethylhexanoate is not thought to be the actual initiator since the molecular weight does not depend on the monomer-to-tin(II) 2-ethylhexanoate molar ratio. Investigations of the coordination–insertion mechanism have resulted in two slightly different reaction pathways. Kricheldorf and co-workers have proposed a mechanism[120] where the monomer and the alcohol added as co-initiator are both coordinated to tin(II) 2-ethylhexanoate during propagation (Scheme 5). Penczek and coworkers have presented a mechanism[121] where tin(II) 2-ethylhexanoate is converted into a tin alkoxide before complexing and ring-opening of the monomer (Scheme 6). Direct observation of the tin alkoxide was achieved by MALDI-TOF spectroscopy for both lactide and ε-caprolactone polymerization.[119]

The tin(II) 2-ethylhexanoate catalyst is a strong transesterification agent, and the resulting copolymers have a randomized microstructure.[122] An increase in reaction temperature or reaction time increases the amount of transesterification reactions. The ROP of lactide with tin(II) 2-ethylhexanoate is fairly slow and it is desirable for economic and commercial reasons to increase the rate of polymerization. The addition of an equimolar amount of triphenylphosphine increases the rate and, as an additional advantage, delays the occurrence of the undesirable backbiting reactions.[123] Recently, bismuth(III) hexanoate has also been used as transesterification catalyst, though in comparison to tin(II) 2-ethylhexanoate, it is less efficient.[124] Whereas blocky sequences of caprolactone units are formed with tin(II) 2-ethylhexanoate as initiator, bismuth(III) hexanoate yield random copolymers.[124]

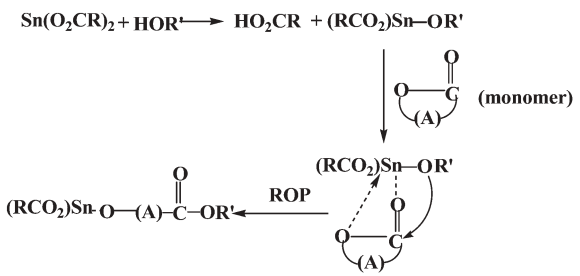

Scheme 6 Coordination-insertion mechanism of ROP by tin(II) 2-ethylhexanoate as proposed by Penczek and co-workers.[121]

In addition to these catalytic applications, medium chain metal alkanoates are also used as (i) primary, secondary and auxiliary driers in alkyd paints,[12] (ii) corrosion protecting reagents,[125] and (iii) biologically active compounds.[18]

6 Conclusions and looking ahead

In this review an attempt has been made to present collectively the different aspects of medium sized metal alkanoates, with a special attention given to 2-ethylhexanoates. In view of their properties such as high solubility in organic solvents, air-stability, wet ability, viscosity, photoactivity, non-toxicity, relatively easy decomposability and also easy availability, these medium chain metal alkanoates are rapidly emerging as extremely attractive precursors for the preparation of ceramic materials by CSD methods. Recent advances in this field have shown excellent applicability of this class of compounds, especially metal 2-ethylhexanoates in obtaining nano-materials by MOD, PMOD or even sol–gel processes. These metal alkanoates are precursors beyond oxides, which have also been used to obtain nanoparticles of metal halides, sulfides, tellurides, *etc.* In addition, metal 2-ethylhexanoates are amongst the most promising catalysts for the ROP of lactones and lactides. Concerted efforts initiated recently to elucidate the chemistry of the manifold applications of medium chain metal alkanoates are enhancing the efficacy of such applications.

Despite of advancements in the chemistry and applications of metal alkanoates, some areas still remain to be explored further. Heterometallic alkanoate derivatives with medium carbon chains is clearly one of those areas, which needs to be explored further due to their potential applications as single source precursors. In this regard, the alkanoate–alkoxide approach has potential to play an important role. It overcomes many shortcomings of all-alkoxide approach such as non-reactivity or absence of correct stoichiometry and is quite helpful in getting desired heterometallics. However, this approach has so far been applied for only selected metals (group 2 and 4 metals, cadmium, lead, *etc.*) and should be extended to other elements. This should be of interest in the case of metals such as lanthanides, lead, bismuth, *etc.* for which cost-efficient synthesis of 2-ethylhexanoates from the metal oxides are available. Moreover, most alkoxides of bismuth are difficult to synthesize and handle because of their light-, heat- and air-sensitivity, and which are also known to be inert with other metal alkoxides.

Better knowledge of the structural properties of precursors based on X-ray studies facilitates molecular design of the precursors. X-Ray characterized 2-ethylhexanoate and other higher alkanoate derivatives are still scarce because of the obvious problem of obtaining crystals of good quality (long carbon chains favour disorder). Predicting the MM′ stoichiometry remains difficult for mixed alkanoate–alkoxide heterometallics due to a lack of structural data. With tremendous advancement in the single-crystal X-ray crystallography technique, attempts should now be made to characterize medium chain alkanoates of metals, which are important from a materials science point of view.

Polynuclear oxo or hydroxo aggregates of large oxophilic metals wrapped in small chain alkanoate groups (mainly based

on acetic or benzoic acids) have attracted considerable attention due to their properties such as single molecule magnets (SMMs). These studies should be extended with medium sized alkanoates also. Exploiting structurally characterized precursors based on the same metal but with different nuclearity for formation of nanoparticles, and isolation of intermediates, should give insight into relationships between the structural features of the precursors and the particles morphology. Such information is nearly nonexistent. The importance of an integrated approach involving synthetic chemistry, physical chemistry, and chemical engineering has emerged for materials science. Emphasis needs to be placed on a better knowledge of thermal or photochemical decomposition pathways of metal alkanoates under various atmospheres and also in *in situ* conditions. As the demands for organization of the solid increase, a more integrated, multidisciplinary approach is also desirable for CSD. The control of the elaboration of nanostructured solids will be a challenge for molecular chemistry.

Abbreviations

AFM	Atomic Force Microscopy
apy	Aminopyridine
BET	Brunauer–Emmett–Teller
bipy	Bipyridine
BST	$Ba_{0.65}Sr_{0.35}TiO_3$
CSD	Chemical Solution Deposition
CVD	Chemical Vapour Deposition
DTA	Differential Thermal Analysis
DMSO	dimethyl sulfoxide
EELS	Electron Energy Loss Spectroscopy
ES	Emission Spectroscopy
ESI-MS	Electro-Spray Ionization Mass Spectrometry
FSP	Flame Spray Pyrolysis
FT-IR	Fourier Transform Infrared Spectroscopy
HRTEM	High Resolution Transmission Electron
HTcS	High T_c Superconductor
ITO	Indium Tin Oxide
LMCT	Ligand to Metal Charge Transfer
LAO	$LaAlO_3$
MALDI-TOF-MS	Matrix Assisted Laser Desorption/ Ionisation Time-of-Flight Mass Spectrometry
MS	Mass Spectrometry
NMR	Nuclear Magnetic Resonance
OAM	Optical Absorption Microscopy
PL	Photo Luminescence
phen	Phenanthroline
py	Pyridine
PZT	$PbZr_{0.53}Ti_{0.43}O_3$
RABiTS	Rolling Assisted Biaxially Textured Substrate
RBS	Rutherford Backscattering Spectrometry
RPO	Ring Opening Polymerization
SBN	$SrBi_2Nb_2O_9$
SBT	$SrBi_2Ta_2O_9$
SEM	Scanning Electron Microscopy
SI-MS	Secondary Ion Mass Spectrometry
STO	$SrTiO_3$
TEM	Transmission Electron Microscopy
THF	Tetrahydrofuran
TGA	Thermo-Gravimetric Analysis
UV-Vis	Ultraviolet-Visible Spectroscopy
XRD	Powder X-Ray Diffraction
XPS	X-Ray Photoelectron Spectroscopy
YAG	Yttrium Aluminate Garnet
YBCO	$YBa_2Cu_3O_{7-x}$

Acknowledgements

S. M. is grateful to Centre National de la Recherche Scientifique (CNRS) for a post-doctoral fellowship.

References

1 (*a*) N. Setter, *J. Eur. Ceram. Soc.*, 2001, **21**, 1279; (*b*) E. Lucas, S. Decker, A. Khaleed, A. Seitz, S. Fultz, A. Ponce, W. Li, C. Carnes and K. J. Klabunde, *Chem. Eur. J.*, 2001, **7**, 2505.
2 (*a*) L. G. Hubert-Pfalzgraf, *Appl. Organomet. Chem.*, 1998, **12**, 221; (*b*) L. G. Hubert-Pfalzgraf, *Coord. Chem. Rev.*, 1998, **178–180**, 967; (*c*) L. G. Hubert-Pfalzgraf, *Inorg. Chem. Commun.*, 2003, **6**, 102.
3 D. C. Bradley, R. C. Mehrotra, I. P. Rothwell and A. Singh, *Metal Alkoxides and Aryloxides*, Academic Press, London, 2001.
4 H. K. Chae, D. A. Payne, Z. Xu and L. Ma, *Chem. Mater.*, 1994, **6**, 1589.
5 L. Ma and D. A. Payne, *Chem. Mater.*, 1994, **6**, 875.
6 L. G. Hubert-Pfalzgraf, S. Daniele, R. Papiernik, M. C. Massiani, B. Septa, J. Vaissermann and J. C. Daran, *J. Mater. Chem.*, 1997, **7**, 753.
7 S. Boulmaaz, R. Papiernik, L. G. Hubert-Pfalzgraf, B. Septe and J. Vaissermann, *J. Mater. Chem.*, 1997, **7**, 2053.
8 A. Brethon, L. G. Hubert-Pfalzgraf and J. C. Daran, *Dalton Trans.*, 2006, 250.
9 A. Brethon and L. G. Hubert-Pfalzgraf, *J. Sol–Gel Sci. Technol.*, 2006, **39**, 159.
10 See, for recent examples: (*a*) M. A. S. Aquino, *Coord. Chem. Rev.*, 2004, **248**, 1025, and references therein; (*b*) A. Grodzicki, I. Lakomska, P. Piszczek, I. Szymanska and E. Szlyk, *Coord. Chem. Rev.*, 2005, **249**, 2232, and references therein.
11 K. M. Stridsberg, M. Ryner and A.-C. Albertsson, *Adv. Polym. Sci.*, 2002, **157**, 41.
12 R.V. Gorkum and E. Bouwman, *Coord. Chem. Rev.*, 2005, **249**, 1709.
13 T. R. Lomar and K. Perera, *Acta Crystallogr., Sect. B*, 1974, **30**, 2912.
14 M. Petric, I. Leban and P. Segedin, *Polyhedron*, 1993, **12**, 1973.
15 N.-E. Ghermani, C. Lecomte, C. Rapin, P. Steinmetz, J. Steinmetz and B. Malaman, *Acta Crystallogr., Sect. B*, 1994, **50**, 157.
16 M. Petric, I. Leban and P. Segedin, *Polyhedron*, 1995, **14**, 983.
17 M. Petric, I. Leban and P. Segedin, *Polyhedron*, 1996, **15**, 4277.
18 B. Kozlevcar, N. Lah, S. Makuc, P. Segedin and F. Pohleven, *Acta Chim. Slov.*, 2000, **47**, 421.
19 M. Rusjan, Z. Chaia, O. E. Piro, D. Guillon and F. D. Cukiernik, *Acta Crystallogr., Sect. B*, 2000, **56**, 666.
20 N. Lah, G. Giester, J. Lah, P. Segedin and I. Leban, *New J. Chem.*, 2001, **25**, 753.
21 N. Lah, P. Segedin and I. Leban, *Struct. Chem.*, 2002, **13**, 357.
22 (*a*) N. Lah, J. Koller, G. Giester, P. Segedin and I. Leban, *New J. Chem.*, 2002, **26**, 933; (*b*) I. Leban, N. Lah and P. Segedin, *Acta Crystallogr., Sect. A*, 2002, **58**, C133.
23 B. Kozlevcar, I. Leban, M. Petric, S. Petricek, O. Roubeau, J. Reedijk and P. Segedin, *Inorg. Chim. Acta*, 2004, **357**, 4220.
24 S. T. Warzeska, M. Zonneveld, R. V. Gorkum, W. J. Muizebelt, E. Bouwman and J. Reedijk, *Prog. Org. Coat.*, 2002, **44**, 243.
25 (*a*) K. Binnemans, P. Martello, I. Couwenberg, H. D. Leebeeck and C. Gorller-Walrand, *J. Alloys Compd.*, 2000, **303–304**, 387;

(*b*) K. Binnemans, L. Jongen, C. Bromant, D. Hinz and G. Meyer, *Inorg. Chem.*, 2000, **39**, 5938.
26 (*a*) L. Jongen, K. Binnemans, D. Hinz and G. Meyer, *Liq. Cryst.*, 2001, **28**, 819; (*b*) K. Binnemans, B. Heinrich, D. Guillon and D. W. Bruce, *Liq. Cryst.*, 1999, **26**, 1717.
27 J. Peultier, M. Francois and J. Steinmetz, *Acta Crystallogr., Sect. C*, 1999, **55**, 2064.
28 F. Lacouture, J. Peultier, M. Francois and J. Steinmetz, *Acta Crystallogr., Sect. C*, 2000, **56**, 556.
29 (*a*) F. Lacouture, M. Francois, C. Didierjean, J.-P. Rivera, E. Rocca and J. Steinmetz, *Acta Crystallogr., Sect. C*, 2001, **57**, 530; (*b*) H. A. Ellis, N. A. S. White, R. A. Taylor and P. T. Maragh, *J. Mol. Struct.*, 2005, **738**, 205.
30 L. Jongen, C. Bromant, D. Hinz-Hubner, G. Meyer, K. Robeyns, K. V. Hecke, L. V. Meervelt and K. Binnemans, *Z. Anorg. Allg. Chem.*, 2003, **629**, 975.
31 M. A. Poraikoshits, A. S. Antsyshkina, G. G. Sadikov, E. N. Lebedeva, S. S. Korovin, R. N. Shchelokov and V. G. Lebedev, *Russ. J. Inorg. Chem.*, 1995, **40**, 748.
32 M. Francois, M. I. Saleh, P. Rabu, M. Souhassou, B. Malaman and J. Steinmetz, *Solid State Sci.*, 2005, **7**, 1236.
33 D. V. Baxter, R. H. Cayton, M. H. Chisholm, J. C. Huffman, E. F. Putilina, S. L. Tagg, J. L. Wesemann, J. W. Zwanziger and F. D. Darrington, *J. Am. Chem. Soc.*, 1994, **116**, 4551.
34 F. Micciche, M. A. V. Straten, W. Ming, E. Oostveen, J. V. Haveren, R. V. D. Linde and J. Reedijk, *Int. J. Mass Spectrom.*, 2005, **246**, 80.
35 A. S. Shaikh and G. M. Vest, *J. Am. Ceram. Soc.*, 1986, **69**, 682.
36 A. Doyle, J. Felcman, M. T. D. P. Gambardella, C. N. Verani and M. L. B. Tristao, *Polyhedron*, 2000, **19**, 2621.
37 (*a*) R. A. Taylor, H. A. Ellis, P. T. Maragh and N. A. S. White, *J. Mol. Struct.*, 2006, **787**, 113; (*b*) P. Segedin, N. Lah, M. Zefran, I. Leban and L. Golic, *Acta Chim. Slov.*, 1999, **46**, 173.
38 O. Berkesi, I. Dreveni, J. A. Andor and J. Mink, *Inorg. Chim. Acta*, 1992, **195**, 169.
39 S. M. Lala, L. A. Montoro, E. D. Donato and J. M. Rosolen, *J. Power Sources*, 2003, **114**, 127.
40 T. R. Lomar and K. Perera, *Acta Crystallogr., Sect. B*, 1974, **30**, 2913.
41 L. Bonnet, F. D. Cukiernik, P. Maldivi, A.-M. Giroud-Godquin, J.-C. Marchon, M. Ibn-Elhaj, D. Guillon and A. Skoulios, *Chem. Mater.*, 1994, **6**, 31.
42 F. D. Cukiernik, M. Ibn-Elhaj, Z. D. Chaia, J.-C. Marchon, A.-M. Giroud-Godquin, D. Guillon, A. Skoulios and P. Maldivi, *Chem. Mater.*, 1998, **10**, 83.
43 M. Bardet, P. Maldivi, A.-M. Giroud-Godquin and J.-C. Marchon, *Langmuir*, 1995, **11**, 2306.
44 O. Poizat, D. P. Strommen, P. Maldivi, A.-M. Giroud-Godquin and J.-C. Marchon, *Inorg. Chem.*, 1990, **29**, 4851.
45 V. Kumar, I. Packiaselvam, K. Sivanandan, M. A. Vahab and A. K. Sinha, *J. Am. Ceram. Soc.*, 2006, **89**, 1136.
46 X. Zhang and R. H. Hill, *J. Photopolym. Sci. Technol.*, 2006, **19**, 477.
47 N. Kumar, D. G. Tuck and K. D. Watson, *Can. J. Chem.*, 1987, **65**, 740.
48 E. P. Kovsman, M. I. Yanovskaya, B. G. Soldatov and G. V. Mozak, *US Pat.*, 6033551 A 20000307, 2000.
49 N. Lah, G. Rep, P. Segedin, L. Golic and I. Leban, *Acta Crystallogr., Sect. C*, 2000, **56**, 642.
50 (*a*) C.-C. Wu, S. A. Hunt, P. K. Gantzel, P. Gutlich and D. N. Hendrickson, *Inorg. Chem.*, 1997, **36**, 4717; (*b*) T. Nakamoto, M. Hanaya, M. Katada, K. Endo, S. Kitagawa and H. Sano, *Inorg. Chem.*, 1997, **36**, 4347.
51 J. Li, C. Huang, B. Li and G. Xu, *Gaodeng Xuexiao Huaxue Xuebao*, 1990, **11**, 226.
52 F. D. Cukiernik, D. Luneau, J.-C. Marchon and P. Maldivi, *Inorg. Chem.*, 1998, **37**, 3698.
53 A. Zelcer, Z. D. Chaia, F. D. Cukiernik, E. E. Castellano and O. E. Piro, *Acta Crystallogr., Sect. C*, 2002, **58**, m144.
54 (*a*) G. B. Deacon and R. J. Phillips, *Coord. Chem. Rev.*, 1980, **33**, 227; (*b*) K. Nakamoto, *Infrared and Raman Spectra of Inorganic and Coordination Compounds*, John Wiley, New York, 4th edn, 1986.
55 A. Labouriau, D. Taylor, T. S. Stephens and M. Pasternak, *Polym. Degrad. Stab.*, 2006, **91**, 1896.
56 F. Micciche, G. J. Long, A. M. Shahin, F. Grandjean, W. Ming, J. V. Haveren and R. V. D. Linde, *Inorg. Chim. Acta*, 2007, **360**, 535.
57 (*a*) S. Morlens, L. Ortega, B. Rousseau, S. Phok, J. L. Deschanvre, P. Chaudouet and P. Odier, *Mater. Sci. Eng., B*, 2003, **104**, 185; (*b*) B. Rousseau, S. Phok, L. Ortega, N. Guibadj, T. Wegelius, S. Morlens, P. Odier, F. Weiss and J. Eikmeyer, *J. Eur. Ceram. Soc.*, 2005, **25**, 2185; (*c*) E. Stewart, M. S. Bhuiyan, S. Sathyamurthy and M. Paranthaman, *Mater. Res. Bull.*, 2006, **41**, 1063.
58 W.-N. Shen, B. Dunn, C. D. Moore, M. S. Goorsky, T. Radetic and R. Gronsky, *J. Mater. Chem.*, 2000, **10**, 657.
59 D. V. Baxter, M. H. Chisholm, M. A. Lynn and E. F. Putilina, *Chem. Mater.*, 1998, **10**, 1758.
60 J. A. R. Cheda, M. V. Garcia, M. I. Redondo, S. Gargani and P. Ferloni, *Liq. Cryst.*, 2004, **31**, 1.
61 M. Ibn-Elhaj, D. Guillon, A. Skoulion, P. Maldivi, A.-M. Giroud-Godquin and J. C. Marchon, *J. Phys. (Paris) II*, 1992, **2**, 2237.
62 See, for example: (*a*) A.-M. Giroud-Godquin, *Coord. Chem. Rev.*, 1998, **178–180**, 1485; (*b*) K. Binnemans, *Chem. Rev.*, 2005, **105**, 4148.
63 T. Maruyama and T. Nakai, *Appl. Phys. Lett.*, 1991, **58**, 2079.
64 W. B. Carter, G. W. Book, T. A. Polley, D. W. Stollberg and J. M. Hampikan, *Thin Solid Films*, 1999, **347**, 25.
65 (*a*) S. Xue, W. Ousi-Benomar and R. A. Lessard, *Thin Solid Films*, 1994, **250**, 194; (*b*) I. Yamaguchi, T. Terayama, S. Ohnishi, T. Manabe, T. Shimizu, T. Kumagai and S. Mizuta, *Thin Solid Films*, 2001, **391**, 157.
66 Y. Sato, M. Ando and K. Murai, *Solid State Ionics*, 1998, **113–115**, 443.
67 C.-C. Kei, K.-H. Kuo, C.-Y. Su, C.-T. Lee, C.-N. Hsiao and T.-P. Pemg, *Chem. Mater.*, 2006, **18**, 4544.
68 M. Epifani, R. Diaz, J. Arbiol, P. Siciliano and J. Morante, *Chem. Mater.*, 2006, **18**, 840.
69 M. Ando, T. Kobayashi, S. Iijima and M. Haruta, *J. Mater. Chem.*, 1997, **7**, 1779.
70 A.-D. Li, C.-Z. Ge, D. Wu, P. Lu, Y.-Q. Zuo, S.-Z. Yang and N.-B. Ming, *Thin Solid Films*, 1997, **298**, 165.
71 J. D. Vyas and K.-L. Choy, *Mater. Sci. Eng., A*, 2000, **277**, 206.
72 U. Hasenkox, S. Hoffmann and R. Waser, *J. Sol–Gel Sci. Technol.*, 1998, **12**, 67.
73 (*a*) P. A. Langjahr, T. Wagner, M. Ruhle and F. F. Lange, *Mater. Res. Soc. Symp. Proc.*, 1996, **401**, 109; (*b*) P. A. Langjahr, F. F. Lange, T. Wagner and M. Ruhle, *Acta Mater.*, 1998, **46**, 773.
74 C.-L. Sun, H.-W. Wang, M.-C. Chang, M.-S. Lin and S.-Y. Chen, *Mater. Chem. Phys.*, 2002, **78**, 507.
75 S. B. Singh, H. B. Sharma, H. N. K. Sharma and S. Phanjoubam, *Ferroelectr. Lett.*, 2006, **33**, 83.
76 Y. T. Kwon, L.-M. Lee, W. I. Lee, C. J. Kim and I. K. Yoo, *Mater. Res. Bull.*, 1999, **34**, 749.
77 Y.-C. Lin, C.-H. Chou, N.-H. Tai, J.-H. Huang and I.-N. Lin, *Integr. Ferroelectr.*, 2004, **64**, 237.
78 S.-Y. Chen and V.-C. Lee, *J. Appl. Phys.*, 2000, **87**, 8024.
79 S.-Y. Chen, B.-C. Lan, C.-S. Taso and S.-Y. Lee, *J. Non-Cryst. Solids*, 2003, **320**, 76.
80 C.-H. Lu and C.-Y. Wen, *J. Eur. Ceram. Soc.*, 2000, **20**, 739.
81 A. A. Avey and R. H. Hill, *J. Am. Chem. Soc.*, 1996, **118**, 237.
82 R. Cordova, H. Gomez, R. Schrebler, P. Cury, M. Orellana, P. Grez, D. Leinen, J. R. Ramos-Barrado and R. D. Rio, *Langmuir*, 2002, **18**, 8647.
83 W. L. Law and R. H. Hill, *Mater. Res. Bull.*, 1998, **33**, 69.
84 L. S. Andronic and R. H. Hill, *J. Photochem. Photobiol., A: Chemistry*, 2002, **152**, 259.
85 H. J. Zhu and R. H. Hill, *J. Non-Cryst. Solids*, 2002, **311**, 174.
86 S. Trudel, G. Li, X. Zhang and R. H. Hill, *J. Photopolym. Sci. Technol.*, 2006, **19**, 467.
87 Y. Miyamoto, T. Tsuchiya, I. Yamaguchi, T. Manabe, H. Niino, A. Yabe, T. Kumagai, T. Tsuchiya and S. Mizuta, *Appl. Surf. Sci.*, 2002, **197–198**, 398.
88 H.-H. Park, S. Yoon, H.-H. Park and R. H. Hill, *Thin Solid Films*, 2004, **447–448**, 669.
89 L. S. Hung and L. R. Zheng, *Appl. Phys. Lett.*, 1992, **60**, 2210.

90 C. Savaniu, A. Arnautu, C. Cobianu, G. Craciun, C. Flueraru, M. Zaharescu, C. Parlog, F. Paszti and A. V. D. Berg, *Thin Solid Films*, 1999, **349**, 29.
91 T.-J. Zhang, H. Ni and W. Wang, *J. Mater. Synth. Process.*, 2002, **10**, 17.
92 P. K. Sharma, G. L. Messing and D. K. Agrawal, *Thin Solid Films*, 2005, **491**, 204.
93 B. E. Watts, F. Leccabue, M. Fanciulli, S. Ferrari and G. Tallarida, *Mater. Sci. Semicond. Process.*, 2003, **5**, 147.
94 C. Legrand, J. H. Yi, P. Thomas, R. Guinebretiere and J. P. Mercurio, *J. Eur. Ceram. Soc.*, 1999, **19**, 1379.
95 G. Rodriguez-Gattorno, D. Diaz, L. Rendon and G. O. Hernandez-Segura, *J. Phys. Chem. B*, 2002, **106**, 2482.
96 R. N. Grass and W. J. Stark, *J. Mater. Chem.*, 2006, **16**, 1825.
97 (*a*) L. R. Alden, D. K. Han, F. Matsumoto, H. D. Abruna and F. J. DiSalvo, *Chem. Mater.*, 2006, **18**, 5591; (*b*) L. R. Alden, C. Roychowdhury, F. Matsumoto, D. K. Han, V. B. Zeldovich, H. D. Abruna and F. J. DiSalvo, *Langmuir*, 2006, **22**, 10465.
98 S. Music, D. Dragcevic, S. Popovic and M. Ivanda, *Mater. Lett.*, 2005, **59**, 2388.
99 M. Ristic, S. Music, M. Ivanda and S. Popovic, *J. Alloys Compd.*, 2005, **397**, L1.
100 M. Epifani, J. Arbiol, R. Diaz, M. J. Peralvarez, P. Siciliano and J. R. Morante, *Chem. Mater.*, 2005, **17**, 6468.
101 Y. J. Kim, Y. S. Kim, S. Y. Chai, D. H. Cha, Y. S. Choi and W. I. Lee, *New J. Chem.*, 2007, **31**, 260.
102 A. Chiorino, G. Ghiotti, F. Prinetto, M. C. Carotta, D. Gnani and G. Martinelli, *Sens. Actuators, B*, 1999, **58**, 338.
103 K. V. P. M. Shafi, A. Ulman, J. Lai, N.-L. Yang and M.-H. Cui, *J. Am. Chem. Soc.*, 2003, **125**, 4010.
104 A. Camenzind, R. Strobel and S. E. Pratsinis, *Chem. Phys. Lett.*, 2005, **415**, 193.
105 J. Marchal, T. John, R. Baranwal, T. Hinklin and R. M. Laine, *Chem. Mater.*, 2004, **16**, 822.
106 K. Kato, K. Suzuki, K. Tanaka, D. Fu, K. Nishizawa and T. Miki, *Integr. Ferroelectr.*, 2004, **62**, 133.
107 L. Nibou, A. Aftati, M. E. Farissi and J.-P. Mercurio, *J. Eur. Ceram. Soc.*, 1999, **19**, 1383.
108 R. N. Grass and W. J. Stark, *Chem. Commun.*, 2005, 1767.
109 M.-R. Song and Z.-J. Zhang, *Mater. Lett.*, 2004, **58**, 2049.
110 D. Diaz, M. Rivera, T. Ni, J.-C. Rodriguez, S.-E. Castillo-Blum, D. Nagesha, J. Robles, O.-J. Alvarez-Fregoso and N. A. Kotov, *J. Phys. Chem. B*, 1999, **103**, 9854.
111 W. Lu, Y. Ding, Y. Chen, Z. L. Wang and J. Fang, *J. Am. Chem. Soc.*, 2005, **127**, 10112.
112 S. Sabata and J. Hetflejs, *J. Appl. Polym. Sci.*, 2002, **85**, 1185.
113 F. Micciche, J. V. Haveren, E. Oostveen, W. Ming and R. V. D. Linde, *Appl. Catal. A: Gen.*, 2006, **297**, 174–181.
114 D. B. Gorman and I. A. Tomlinson, *Chem. Commun.*, 1998, 25.
115 H. R. Kricheldorf, G. Behnken and G. Schwarz, *Polymer*, 2005, **46**, 11219.
116 (*a*) M. Hans, P. Gasteier, H. Keul and M. Moeller, *Macromolecules*, 2006, **39**, 3184; (*b*) H. R. Kricheldorf, I. Kreiser-Saunders and D.-O. Damrau, *Macromol. Symp.*, 2000, **159**, 247.
117 Y. Jang, H.-K. Sung and H. Kwag, *Eur. Polym. J.*, 2006, **42**, 1250.
118 See for example,(*a*) H. R. Kricheldorf and J. Meier-Haack, *Macromol. Chem.*, 1993, **194**, 715; (*b*) A.-C. Albertsson and M. Gruvegard, *Polymer*, 1995, **36**, 1009; (*c*) S. Huijser, B. B. P. Staal, J. Huang, R. Duchateau and C. E. Koning, *Angew. Chem., Int. Ed.*, 2006, **45**, 4104.
119 A. Kowalski, A. Duda and S. Penczek, *Macromolecules*, 2000, **33**, 7359.
120 (*a*) H. R. Kricheldorf, I. Kreiser-Saunders and C. Boettcher, *Polymer*, 1995, **36**, 1253; (*b*) H. R. Kricheldorf, I. Kreiser-Saunders and A. Stricker, *Macromolecules*, 2000, **33**, 702.
121 A. Kowalski, A. Duda and S. Penczek, *Macromol. Rapid Commun.*, 1998, **19**, 567.
122 M. Bero, B. Czapla, P. Dobrzynski, H. Janeczek and J. Kasperczyk, *Macromol. Chem. Phys.*, 1999, **200**, 911.
123 P. Degee, P. Dubois, S. Jacobsen, H.-G. Fritz and R. Jerome, *J. Polym. Sci., Polym. Chem.*, 1999, **37**, 2413.
124 H. R. Kricheldorf, K. Bornhorst and H. Hachmann-Thiessen, *Macromolecules*, 2005, **38**, 5017.
125 (*a*) E. Rocca and J. Steinmetz, *Corros. Sci.*, 2001, **43**, 891; (*b*) D. Daloz, C. Rapin, P. Steinmetz and G. Michot, *Corrosion*, 1998, **54**, 444.